Journal of Neurochemistry, 2004, **90**, 142–154 doi:10.1111/j.1471-4159.2004.02470.x

Mapping spatio-temporal activation of Notch signaling during neurogenesis and gliogenesis in the developing mouse brain

Akinori Tokunaga,*,†,‡ Jun Kohyama,* Tetsu Yoshida,* Keiko Nakao,*,† Kazunobu Sawamoto*,† and Hideyuki Okano*,†

**Department of Physiology, Keio University School of Medicine, Tokyo, Japan*

†Core Research for Evolutional Science and Technology (CREST), Japan Science and Technology Agency, Saitama, Japan

‡Osaka University Graduate School of Medicine, Suita, Osaka, Japan

Abstract

Notch1 plays various important roles including the maintenance of the stem cell state as well as the promotion of glial fates in mammalian CNS development. However, because of the very low amount of the activated form of Notch1 present *in vivo*, its precise activation pattern has remained unknown. In this study, we mapped the active state of this signaling pathway *in situ* in the developing mouse brain using a specific antibody that recognizes the processed form of the intracellular domain of Notch1 cleaved by presenilin/γ-secretase activity. By using this antibody, active state of Notch1 came to be detectable with a higher sensitivity than using conventional antibody against Notch1. We found that activated Notch1 was mainly detected in the nuclei of a subpopulation of radial glial cells, the majority of proliferating precursor cells in the ventricular zone (VZ). However, Notch1 activation was not detected in neuronal precursor cells positive for neuronal basic helix-loop-helix proteins or in differentiating neurons in the embryonic forebrain. Interestingly, we found that Notch1 was transiently activated in the astrocytic lineage during perinatal CNS development. Taken together, the present method has enabled us to determine the timing, gradients, and boundaries of the activation of Notch signaling.

Keywords: activated Notch1, gliogenesis, Mash1, neurogenesis, neurogenin2, radial glia.

J. Neurochem. (2004) **90**, 142–154.

During mammalian CNS development, neurons and glia are generated from common neural progenitor cells [multipotent neural stem cells (NSCs)] (Qian *et al.* 2000; Anderson 2001; Okano 2002; Sun *et al.* 2003). In this process, Notch signaling regulates the differentiation state of NSCs in a context-dependent manner (Beatus and Lendahl 1998; Artavanis-Tsakonas *et al.* 1999; Gaiano and Fishell 2002). When Notch receptors (Notch1–4 in vertebrates) (Weinmaster *et al.* 1991) are activated by their ligands, encoded by the Delta/Serrate/lag-2 (DSL) genes, the intracellular domain (ICD) of Notch is cleaved by presenilin/γ-secretase (Selkoe and Kopan 2003). The Notch1-ICD (N1-ICD) then translocates into the nucleus to form a complex with CSL (CBF1/RBP-J in mammals) (Kato *et al.* 1997) and activates the transcription of the basic helix-loop-helix (bHLH) genes *Hes1* and *Hes5*, which act as downstream effectors of Notch (de la Pompa *et al.* 1997; Kageyama and Nakanishi 1997; Nakamura *et al.* 2000; Ross *et al.* 2003). Hes1 and Hes5 repress the expression of proneural bHLH genes such as *Mash1* (Ishibashi *et al.* 1995). The proneural bHLH factors (e.g. Mash1, Neurogenin1 and Neurogenin2) are likely to be involved in the transition from NSC to progenitor cell (Torii *et al.* 1999; Nieto *et al.* 2001; Sun *et al.* 2001). Thus, the activation of Notch signaling inhibits neuronal commitment in the cells that receive it.

Received November 13, 2003; revised manuscript received January 10, 2004; accepted February 20, 2004.

Address correspondence and reprint requests to H. Okano, Department of Physiology, Keio University School of Medicine, 35 Shinanomachi, Shinjuku-ku, Tokyo 160–8582, Japan.
E-mail: hidokano@sc.itc.keio.ac.jp

Abbreviations used: bHLH, basic helix-loop-helix; BLBP, brain lipid binding protein; DMEM, Dulbecco's modified Eagle's medium; DSL, Delta/Serrate/lag-2; GE, ganglionic eminence; GFAP, glial fibrillary acidic protein; GS, glutamine synthetase; ICD, intracellular domain; IR, immunoreactivity; LGE, lateral ganglionic eminence; N1-ICD, Notch1-ICD; NSC, neural stem cell; PBS, phosphate buffered saline; PCNA, proliferating cell nuclear antigen; PFA, paraformaldehyde; SDS–PAGE, sodium dodecyl sulfate–polyacrylamide gel electrophoresis; VZ, ventricular zone.

Notch1-mediated signal pathways play crucial roles in mammalian CNS development, including in maintenance of a neural stem cell (progenitor) state, inhibition of neuronal commitment, and promotion of glial fates (Wang and Barres 2000; Gaiano and Fishell 2002). Correspondingly, Notch1 is expressed predominantly in proliferating neural progenitor cells in the ventricular zone (VZ) of the embryonic brain (Lindsell *et al.* 1996), and continues to be expressed postnatally in specific regions. However, the activation pattern of Notch1 during neural development for the most part remains unknown, because only very small amounts of N1-ICD are active, and hardly any is detectable in the nucleus *in vivo* (Schroeter *et al.* 1998).

Here, to determine the activation pattern of Notch signaling *in situ*, we performed immunohistochemical analyses of the embryonic and perinatal mouse brain using an antibody specific for the activated form of Notch1, which enhanced the sensitivity of the detection. We found that in the embryonic mouse forebrain, Notch1 was activated in proliferating neural progenitor cells, but not in postmitotic neurons. In the postnatal brain, it was shown that Notch1-activation took place transiently during the astrocytic development.

Materials and methods

Animals and tissue preparation

C57/BL6 mice, used for the preparation of tissue protein extracts and tissue sections, were obtained from Charles River Japan Inc (Kanagawa, Japan). The date of conception was established by the presence of a vaginal plug and recorded as E0.5; the day of birth was designated as postnatal day (P) 0.

cDNA expression constructs

The forms of mouse Notch1 used in this study are summarized in Fig. 1. The expression vector containing mouse full-length Notch1 was kindly provided by Dr J. Nye. N1ΔE was kindly provided by Dr Masato Nakafuku (Yamamoto *et al.* 2001). These cDNAs were subcloned into the pEF-Bos expression vector.

Transfection of cultured cells

The NIH3T3 mouse fibroblast cell line was maintained at 37°C in 5% CO_2. In transient-expression studies, these cells were transfected with cDNAs inserted into pEF-Bos expression vector using the Lipofectamine Plus reagent (Invitrogen, Carlsbad, CA, USA). The cell lines were maintained in Dulbecco's modified Eagle's medium (DMEM) supplemented with 10% fetal calf serum. The cells were incubated for 24 h after the transfection.

γ-Secretase inhibitor treatment

A stock solution of L-685458 (Bachem, King of Prussia, PA, USA) in dimethyl sulfoxide was diluted to 10 μM in phosphate buffered saline (PBS) and injected into embryonic mouse forebrain *exo utero* at E14.5. Control embryos were mock injected with PBS containing the same concentration of DMSO carrier alone. A 2 μL volume of the solution in PBS was injected into the lateral ventricle with a microinjector (Eppendorf, Hamburg, Germany), and 2 days later the embryos were dissected, fixed, and used for immunostaining. The *exo utero* surgery was performed according to the available protocol (Saito and Nakatsuji 2001). In the case of the NIH3T3 cell line, 6 h after transfection the medium was changed to DMEM containing 10 μM L-685458, and the cultured cells were incubated for 16 h before being used for immunostaining. The dose–response analysis was done by immunoblotting.

5-Bromo-2′-deoxyuridine (BrdU) labeling *in vivo*

To label the cells in S-phase, BrdU (Sigma) was injected intraperitoneally into pregnant female at a gestational day from E14.5 [100 μg/g body weight in 200 μL of PBS]. At specific intervals following injection (30 min), embryos were dissected from the uterus and fixed with 4% paraformaldehyde (PFA) in PBS overnight.

Antibodies

Commercially available antibodies: Mouse anti-α-tubulin (Sigma-Aldrich, St. Louis, MO, USA), mouse anti-β-tubulin isotype III (Sigma), mouse anti-glial fibrillary acidic protein (GFAP) (Sigma), goat anti-Notch1 (M-20, Santa Cruz Biotechnology, Inc., Santa Cruz, CA, USA), goat anti-Delta (C-20, Santa Cruz), mouse anti-NeuN (Chemicon, Temecula, CA, USA), rabbit anti-Mash1 (Chemicon), mouse anti-proliferating cell nuclear antigen (PCNA) (Oncogene research product, San Diego, CA, USA), mouse anti-Nestin (Rat401, Developmental Studies Hybridoma Bank; DSHB), rabbit anti-Cleaved-Notch1 (actN1) (Cell Signaling, Beverly, MA, USA), mouse anti-phospho-histone3 (Cell Signaling), mouse anti-Ki67 (Novocastra, Newcastle-upon-Tyne, UK), mouse anti-Mash1 (BD Transduction Laboratories, Los Angeles, CA, USA), mouse anti-glutamine synthetase (GS) (BD Transduction Laboratories), sheep anti-BrdU (Fitzgerald Industries International, Inc., Concord, MA, USA). These antibodies were used according to the manufacturer's protocols. Rabbit anti-Hes1 antibody was provided by Dr T. Sudo (Ito *et al.* 2000), rabbit anti brain lipid binding protein (BLBP) antibody was provided by Dr N. Heintz (Feng and Heintz 1995) and mouse anti-Neurogenin2 was provided by Dr DJ Anderson (Lo *et al.* 2002).

Preparation of cell lysates and immunoblotting

Mouse brain was removed from the skull and dissociated in PBS. An equal volume of 2 × sodium dodecyl sulfate–polyacrylamide gel electrophoresis (SDS–PAGE) sample buffer [100 mM Tris-HCl (pH 6.8, 4% SDS, 20% glycerol, 0.02% bromophenol blue, 12% 2-mercaptoethanol] was added to the lysate and the sample was boiled for 5 min. NIH3T3 cells were collected by centrifugation at 100 × *g* for 5 min. The cell pellets were lysed in 1 × SDS–PAGE sample buffer. Equal loading of the lysate proteins was verified by immunoblotting α-tubulin on a duplicate gel. Tissue and cell lysates were resolved on 7.5% SDS–PAGE gels that were then electroblotted onto Immobilon-P membranes (Millipore, Bedford, MA, USA) with a semi-dry transfer apparatus. The chemiluminescent signals were detected by ECL (Amersham Pharmacia Biotech, Piscataway, NJ, USA) with Kodak X-OMAT film (Kodak, Rochester, NY, USA) according to the manufacturer's instructions.

Immunohistochemistry

We performed immunohistochemical study on tissue sections using three or more independent samples from the mice of different

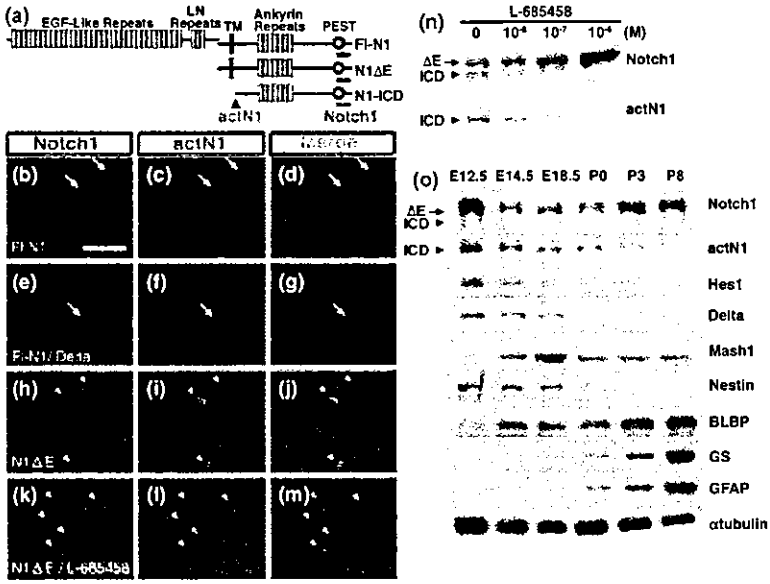

Fig. 1 (a) Schematic representation of the Notch1 protein. cDNAs encoding two forms of Notch1 were assembled: Fl-N1 and N1ΔE. N1-ICD, a form of activated Notch1 processed by S3-site cleavage, is also shown. The respective recognition sites of the anti-Notch1 and actN1 antibodies are also indicated below the schematic drawings. The vertical arrowhead indicates the regions arising from the cleavage. (b–d) NIH3T3 cells that were transfected with Fl-N1 alone showed anti-Notch1-IR (red) in the cell membrane and cytoplasm, but not actN1-IR (green). (e–g) Cells cotransfected with Fl-N1 and Delta showed both Notch1-IR (red) in the cell membrane and cytoplasm, and actN1-IR (green) in the nucleus. (h–j) Cells transfected with N1ΔE, showed strong Notch1 (red) and actN1-IR (green) in the nucleus. (k–m) Cells transfected with N1ΔE and treated with L-685458, a γ-secretase inhibitor, were stained with anti-Notch1-IR (red) but not actN1-IR (green). Nuclei were counterstained with Hoechst (blue). Scale bar: b–m, 50 μm; (n) NIH3T3 cells transfected with N1ΔE were treated with the indicated concentrations of L-685458 for 16 h. Cell lysates were analyzed for N1ΔE (uncleaved) and N1-ICD (cleaved) using the anti-Notch1 and actN1 antibodies. Upper panel, Increasing concentrations of L-685458 led to a build-up of uncleaved Notch1 (120 kDa) by probing the immunoblot with anti-Notch1 antibody. Lower panel, the same fraction was analyzed for the N1-ICD (110 kDa) by sequentially probing the immunoblot with the actN1 antibody. (o) Expression of Notch signaling-related components in the mouse brain. The sizes of N1ΔE (ΔE, arrow) and N1-ICD (ICD, arrowhead) are indicated. α-Tubulin expression was used as a control.

pregnant female. Pups and 8-week-old adult mice were perfused through the left ventricle with 4% PFA in 0.1 M PBS, pH 7.4. Embryos were removed by cesarean section and immediately immersed in the same fixative. Brains were dissected and postfixed overnight at 4°C, cryoprotected in 30% sucrose in PBS overnight at 4°C, then embedded in OCT compound (Tissue Tek; Miles, Elkhart, IN, USA). Cryostat sections (12 μm) were cut and affixed to MAS-coated glass slides (Matsunami Glass, Osaka, Japan). Antigen retrieval was accomplished by autoclave treatment in 0.01 mol/L citrate buffer, pH 6.0, or in Target Retrieval Solution (Dako, Carpinteria, CA, USA), for the anti-Notch1 and Cleaved-Notch1 (actN1) antibodies, at 105°C for 5 min followed by three washes in PBS. The sections were then permeabilized in TBS-T (TBS containing 0.05%Tween20) for 10 min and blocked with 10% normal donkey serum (Chemicon) in PBS for 1 h at room temperature. Subsequently, the sections were incubated overnight at 4°C in a mixture of the primary antibodies described above, in blocking solution. After the sections were washed three times in PBS, they were incubated in a mixture of biotin-conjugated secondary antibodies (Jackson ImmunoResearch, West Grove, PA, USA) for 1 h at room temperature, immersed in 3% H_2O_2 to inactivate endogenous peroxidase at room temperature for 10 min, incubated in the ABC kit mixture (Vector Laboratories, Burlingame, CA, USA), according to the manufacturer's directions, and visualized by the TSA Fluorescein System (PerkinElmer Life sciences, Boston, MA, USA). For double staining, sections were also incubated in a mixture containing the following secondary antibodies for 1 h: Alexa Fluor 488- or 568-conjugated goat anti-mouse, rabbit IgG, or donkey anti-goat IgG (Molecular Probes, Eugene, OR, USA). After being rinsed in PBS, the sections were mounted and examined under a fluorescence microscope (Zeiss Axiophoto) equipped with the appropriate epifluorescence filters. Optical sections were viewed using a scanning-laser confocal imaging system (Zeiss LSM510).

Results

Characterization of Notch1-specific antibodies

To examine the activation patterns of Notch1 *in situ*, we used two commercially available antibodies: anti-Notch1 (M-20) and anti-cleaved Notch1 (actN1). The anti-Notch1 antibody was raised against the C-terminal fragment of the mouse

Notch1 protein, whereas the actN1 antibody recognizes the cleavage site of Notch1, between Gly 1743 and Val 1744, that is generated by presenilin/γ-secretase (see Materials and methods and Fig. 1a). To confirm the specificity of these antibodies, we performed immunocytochemistry and immunoblotting analyses using NIH3T3 cells that were transfected with Notch1 expression vectors.

First, we compared the staining patterns of the actN1 and anti-Notch1 antibodies by immunostaining. NIH3T3 cells were transfected with plasmids encoding full-length mouse Notch1 (Fl-N1) alone or cotransfected with Fl-N1 and Delta (Fig. 1b–g). The anti-Notch1 antibody labeled the cell membrane and cytoplasm of cells that were transfected with Fl-N1 alone but the actN1 antibody did not (Fig. 1b–d), indicating that the Fl-N1 product was not cleaved at the γ-secretase-sensitive site in the absence of an exogenous ligand. However, when NIH3T3 cells were cotransfected with both Fl-N1 and Delta to stimulate Notch signaling in a ligand-dependent manner (Jarriault *et al.* 1998), the major localization sites of Notch1 that were determined by the anti-Notch1 antibody were the cell-membrane and cytoplasm (Fig. 1e), but the cleaved form of Notch1 was detected within the nucleus by the actN1 antibody (Fig. 1f), suggesting that the Fl-N1 product was cleaved in a ligand-dependent manner and then translocated to the nucleus.

To confirm the transactivation of downstream genes by Notch1 in this culture, we introduced a reporter luciferase gene under the control of the *Hes1* promoter (*Hes1*-luc) (Jarriault *et al.* 1995) into NIH3T3 cells by transient transfection. Transactivation of the *Hes1* promoter was observed in cells expressing both Fl-N1 and Delta, but not in cells expressing only Fl-N1 (data not shown). Thus, these results suggest that the expression of both full-length Notch1 and its ligand (Delta) are required for the nuclear localization of activated Notch1 as well as for Hes1-transactivation.

As a positive control, we also analyzed cells transfected with a constitutively active truncated form of Notch1 (N1ΔE) that contained the transmembrane region and the entire ICD. A previous report showed that N1ΔE is a dominant-active form and induces expression of a Notch1 downstream gene (Kopan *et al.* 1996). The N1ΔE products were cleaved by presenilin/γ-secretase in a ligand-independent manner (Fig. 1h-m, described in the next paragraph), producing N1-ICD forms (see Fig. 1a). We also observed the strong transactivation of the *Hes1* promoter in N1ΔE-transfected cells (data not shown). In N1ΔE-transfected cells, Notch1 was clearly detected in the nucleus by both the actN1 (Fig. 1i), and anti-Notch1 (Fig. 1h) antibodies.

To further confirm the specificity of the actN1 antibody for activated Notch1, we investigated the effects of a γ-secretase inhibitor on actN1 immunoreactivity (IR) in NIH3T3 cells transfected with the N1ΔE cDNA. We used a highly specific γ-secretase inhibitor, the L-685458 (Li *et al.* 2000), which blocks Notch endoproteolysis at the γ-secretase-sensitive site. In the presence of this inhibitor, cells transfected with N1ΔE were labeled by the anti-Notch1 antibody but not actN1 antibody (Fig. 1k–m). We also characterized the specificity of the actN1 antibody by immunoblotting. The N1-ICD fragment was readily visible in cells that were not treated with L-685458 by combined immunoblotting with the actN1 and anti-Notch1 antibodies, but the generation of N1-ICD was inhibited by L-685458 treatment (Fig. 1n, upper panel). With increasing concentrations of L-685458, we detected larger amounts of the uncleaved form of Notch1 (120 kDa) with a concomitant decrease in the amount of the cleaved form. Subsequent analysis of the same blot using the actN1 antibody confirmed a dose-dependent reduction in the generation of the cleaved form (110 kDa) by L-685458 treatment (Fig. 1n, lower panel). Collectively, these results show that the actN1 antibody used in the present study can detect the ICD of Notch1 only when it has been cleaved in a γ-secretase-sensitive fashion, but that it does not detect full-length Notch1.

Next, to confirm the specificity of the actN1 antibody for activated Notch1 *in situ*, we investigated the presence of actN1-IR on brain sections obtained at E16.5 from animals that had or had not been injected with γ-secretase inhibitor. In brains injected with PBS alone, nuclear actN1-IR was detected in a subpopulation of the Notch1-IR-positive VZ cells (Fig. 2c,d). The L-685458 treatment did not affect Notch1-IR (Fig. 2e). However, virtually no actN1-IR could be detected in the brain injected with L-685458 (Fig. 2f). These results indicate that the presence of actN1-IR on the brain sections reflects the γ-secretase-dependent activation of Notch1 *in situ*.

Developmental expression of full-length Notch1 and its activated form in the CNS

We, then, examined the activation pattern of Notch1 during mouse brain development by immunoblotting. Uncleaved form of Notch1 (ΔE 120 kDa) was detected from the embryonic stage to the perinatal stage. However, we also detected a strong 110 kDa signal (ICD) in the E12.5 mouse brain using the actN1 antibody, although the activated Notch1 gradually decreased at later stages (Fig. 1o). We also examined the expression of Delta and Hes1 during CNS development. Delta is a Notch ligand and Hes1 is a target of Notch1. They each had almost same expression pattern as activated Notch1 (Fig. 1o). Mash1 is one of the proneural bHLH factors. When cell fate is switched from self-renewal to differentiation, multipotent NSCs generate a transient neuronal precursor cell type, which is defined by the expression of Mash1 (Torii *et al.* 1999). We found that Mash1 showed a complementary expression pattern to activated Notch1 and Hes1, being up-regulated during neurogenesis. Next, we examined the expression patterns of several lineage markers: Nestin, brain lipid binding protein (BLBP), glutamine synthetase (GS), and glial fibrillary acidic

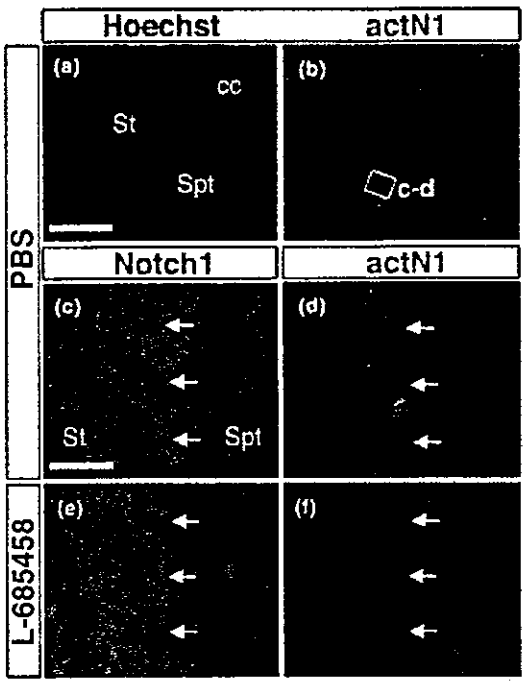

Fig. 2 Characterization of Notch1-specific antibodies by immunohistochemistry. Brain sections at E16.5 were immunostained using anti-Notch1 (red) and actN1 (green) antibodies. (a,b) Activated Notch1 staining (green) was localized to nuclei in the neuroepithelium. This section was counterstained with Hoechst (blue). (c,d) Embryos injected with Mock stained with both anti-Notch1-IR (red) and actN1-IR (green). (e,f) Embryos injected with L-685458 stained with anti-Notch1-IR (red) but not with actN1-IR (green). Arrowheads indicate the ventricle. Striatum (St), septum (Spt) corpus callosum (cc). Scale bars: a,b, 250 μm; c–f, 25 μm.

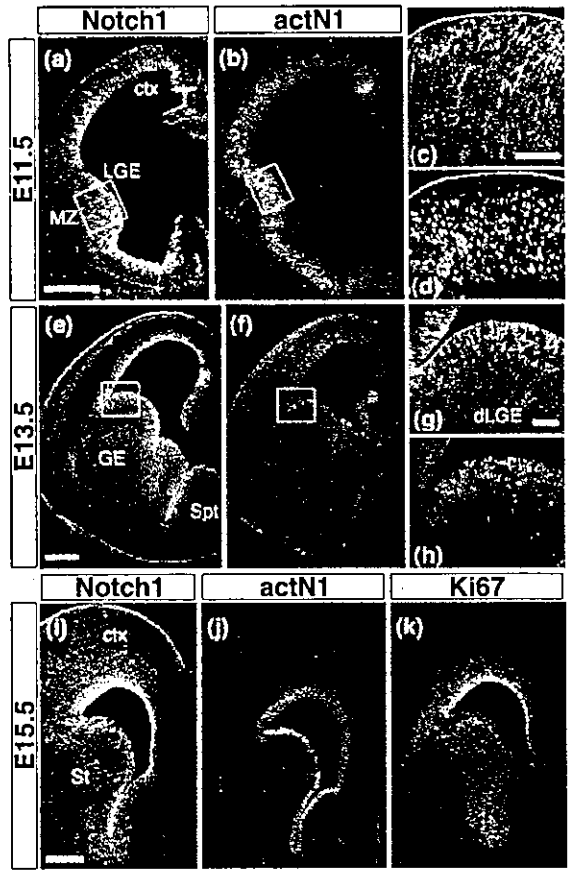

Fig. 3 Immunofluorescence labeling *in situ* throughout the embryonic brain with antibodies against Notch1 (anti-Notch1 and actN1 antibodies). Notch1 was strongly expressed in the neuroepithelium of the basal telencephalic plate, and to a lesser extent in the cortex at E11.5 (a,c) and E13.5 (e,g). Activated Notch1 was localized to the nucleus and strongly expressed in the neuroepithelium of the LGE and septum, but was less strong in the cortex at E11.5 (b,d) and E13.5 (f,h). (i–k) Activated Notch1 was uniformly distributed in anti-Notch1-, anti-Ki67-positive cells in the VZ at E15.5. (c,d) and (g,h) are higher magnification views of the areas boxed in (a,b) and (e,f), respectively. Coronal sections: E11.5 (a–d), E13.5 (e–h), and E15.5 embryos (i–k). Cortex (ctx), lateral ganglionic eminence (LGE), dorsal LGE (dLGE), mantle zone (MZ), striatum (St), septum (Spt). Lateral is to the left, and dorsal is up. Scale bars: a,b, 250 μm; c,d, 50 μm; e,f, 250 μm; g,h, 50 μm; i–k, 250 μm.

protein (GFAP). Nestin is an intermediate filament protein that is expressed in radial glial cells, which have been defined as neural progenitor cells (Hockfield and McKay 1985; Lendahl *et al.* 1990). BLBP is known to be first expressed in radial glial cells, and its expression later becomes restricted to immature astrocytes (Feng *et al.* 1994; Kurtz *et al.* 1994). In the present study, Nestin was expressed during the embryonic stage, but its expression decreased after birth. The expression of BLBP was detected at a later stage than that of Nestin, and BLBP expression gradually increased through the perinatal stage. On the other hand, both astrocyte markers, GS and GFAP, increased with the advancing developmental stage, beginning at around P0 (Fig. 1o).

Next, we used immunohistochemistry to examine the localization of these gene products in the developing brain. Anti-Notch1-IR was found in the VZ of the developing CNS with regional specificity (Fig. 3a,e,i). By E11.5 in the mouse brain, Notch1-IR was strongly detected in the neuroepithelium of the basal telencephalic plate and septum and to a lesser extent in the cortex (Fig. 3a). This is consistent with a previous report of Notch1 expression performed with *in situ* hybridization (Lindsell *et al.* 1996). Moreover, Notch1-IR was localized to the cell membrane (Figs 1b and 3a,c). In contrast, actN1-IR was localized to the nuclei of cells in the VZ at E11.5 (Fig. 3b,d). actN1-IR was strongly detected in the neuroepithelium of the ganglionic eminence (GE) and to a lesser extent in the cortex. Similar to the results for the actN1-immunostaining, a visible difference between the dorsal and ventral telencephalic regions was observed using

anti-Notch1 antibody staining (Fig. 3a,b). However, actN1-IR was not detected at the lumenal surface of the VZ, although the Notch1-IR was strongly detected there (Fig. 3c,d). At E13.5 and E15.5, actN1-positive cells were sparsely distributed among the anti-Notch1-positive cells in the germinal zone of the lateral ganglionic eminence (LGE) and septum (Fig. 3e–j). These results showed that cleavage of Notch1 occurred in a subpopulation of the Notch1-positive proliferating cells in the fetal mouse forebrain. Furthermore, the areas labeled by actN1-IR were part of the Ki67-positive proliferating cells (Fig. 3j,k). At the same stage, actN1-IR was also detected in the midbrain, hindbrain, eye, neural crest, and olfactory epithelium (data not shown).

To examine in more detail the cell types in which Notch1 is activated, we performed double immunohistochemical staining using the actN1 antibody and antibodies against several cell-type-specific markers, followed by comparative confocal microscopic analysis of the cerebral cortex and GE at E11.5 and E14.5. At these stages, Nestin is expressed in the radial glial cells, which are mainly visualized as fibers extending from the ventricular area to the pial surface (Hockfield and McKay 1985; Lendahl *et al.* 1990; Miyata *et al.* 2001; Rakic 2003). Notch1-IR was detected in almost the same area as Nestin (Fig. 4a–c), and the similarity of their localization suggested that the cell membrane was adjacent to the intermediate filaments. Thus, Notch1 is strongly expressed in radial glial cells, In contrast, the actN1-IR-positive cells were a subset of the Nestin- and Notch1-positive cells that lay closer to the ventricular surface (Fig. 4d–g). Nonetheless, the activated Notch1 was not expressed in βIII-tubulin-positive neurons (Fig. 4h). In addition, activated Notch1 labeling was observed in PCNA-positive proliferating cells, within the VZ (Fig. 4i).

It is notable that the actN1-IR was not detected at the lumenal surface of the VZ (Fig. 4j–l), i.e. the site of the mitosis, although the Notch1-IR was present in this area (Fig. 3c,d). Here, we further characterized the Notch1-activation during cell cycle phases. We examined the localization of actNI-IR in the following cell types: (i) the cells labeled by a short (1/2 h) BrdU-pulse that are mostly in S-phase; and (ii) the cells positive for Phospho-histone3 (PH3, a specific marker of mitotic cells), that are in M phase and located at the lumenal surface of the VZ. Interestingly, the actN1-IR correlated with the 1/2 h BrdU-pulse-labeled cells (Fig. 4m), but not with the PH3-positive cells (Fig. 4n) at E14.5. Thus, Notch1 is likely to be activated at least in S phases, but not in M phases. This result indicated that the Notch1-signaling is activated in a cell cycle phase-dependent fashion.

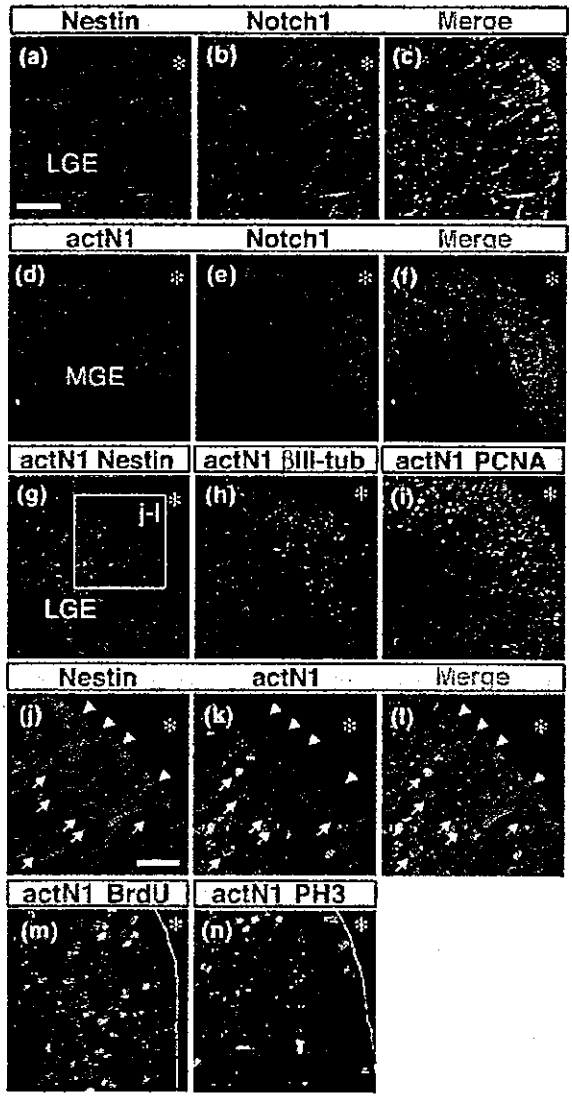

Fig. 4 Expression pattern of activated Notch1 in the developing CNS. (a–c) Brain sections were immunostained using anti-Notch1 (green) and anti-Nestin (red) antibodies. Notch1 was coexpressed with Nestin in the VZ of the basal forebrain. (d–f) Activated Notch1 staining (green) was seen in the Notch1-positive neuroepithelium (red). (g–i), actN1 staining (green) was seen in the Nestin-positive neuroepithelium (g, red). actN1-positive cells were double labeled with PCNA-IR (i, red), but not βIII-tubulin-IR (h, red). (j–l) enlarged image of (g). (m,n) actN1-positive cells were double labeled with BrdU-IR (m, red), but not PH3 (n, red). Arrows depict examples of Nestin- and actN1-double-labeled cells. Arrowheads depict the lumenal surface of the VZ. Coronal sections: E11.5 (a–f), and E14.5 (g–n) embryos. Asterisk: lateral ventricle. Lateral ganglionic eminence (LGE), Medial ganglionic eminence (MGE). Scale bars: a–i, 50 μm; j–n, 25 μm.

Developmental expression of activated Notch1 and proneural bHLH factors (Mash1 or Neurogenin2) in the early embryonic CNS

Regarding the expression of the two proneuronal bHLH factors in the mouse embryonic forebrain, Mash1 has been shown to be expressed at high levels in ventral neuronal progenitors and at reduced levels in a subset of dorsal neuronal progenitors, contrasting the restricted expression of

Neurogenin2 (Ngn2) in dorsal neuronal progenitors (Fode *et al.* 2000). In addition to responding to the specifications of dorsal-ventral identity, Mash1 and Ngn2 are known to have similar roles in neuronal commitment (Nieto *et al.* 2001). The immunoblot analysis in the present study revealed that the expression profile of Mash1 was complementary to that of activated Notch1 (Fig. 1o). Here, we characterized the relationship between Mash1 or Ngn2-expressing cells and actN1-IR positive cells in greater detail using immunohistochemistry.

First, to examine the features of the Mash1-expressing cells, we performed immunostaining with Mash1 and several lineage markers. In the early embryonic telencephalon at E11.5 and E14.5, Mash1 was expressed in the germinal zone of the GE (Fig. 5a,b). Mash1 expression was colocalized with Nestin (Fig. 5c,d), and there was no overlap with βIII-tubulin (Fig. 5e,f), just as seen with the actN1-IR-positive cells (Fig. 4g,h).

Next, to determine the cell types in which Notch1 is activated in the developing brain, we performed double immunohistochemistry staining using the actN1, Mash1 and Ngn2 antibodies. Mash1 and activated Notch1 were expressed in a complementary fashion at E11.5 and E14.5 in the germinal zone of the GE (Fig. 5g–j). Likewise, Ngn2 and activated Notch1 exhibited complementary expression profiles in the germinal layers of the cortex (Fig. 5k–n). Furthermore, Mash1 or Ngn2 were transiently expressed in Nestin-IR-positive and actN1-IR-negative cells, and the number of cells expressing these bHLH proteins were highest in the VZ throughout neural development (Fig. 5g–n). These results suggest that the Nestin-positive precursor cells in the embryonic forebrain can be classified into two populations that are positive for either activated Notch1 or Mash1/Ngn2, but not both.

Notch1 is activated in the generation of astrocytes in the late embryonic CNS

Notch receptors play crucial roles in many cellular differentiation programs. In addition to the more classical role of Notch in keeping cells in an undifferentiated state (Gaiano *et al.* 2000; Chambers *et al.* 2001; Hitoshi *et al.* 2002), a recent paper has provided *in vitro* and *in vivo* evidences indicating that Notch signaling is a powerful means of directing CNS precursor cells into the glial fate (Gaiano *et al.* 2000; Nye *et al.* 1994; Tanigaki *et al.* 2001).

Therefore, we examined whether Notch1 is activated endogenously in the cells of the astrocytic lineage within the peri-ventricular area at E17.5, P0, and P8, when a high level of gliogenesis occurs (Alvarez-Buylla *et al.* 2001). In recent years, several reports have described the transition from radial glia to astrocytes (Schmechel and Rakic 1979; Voigt

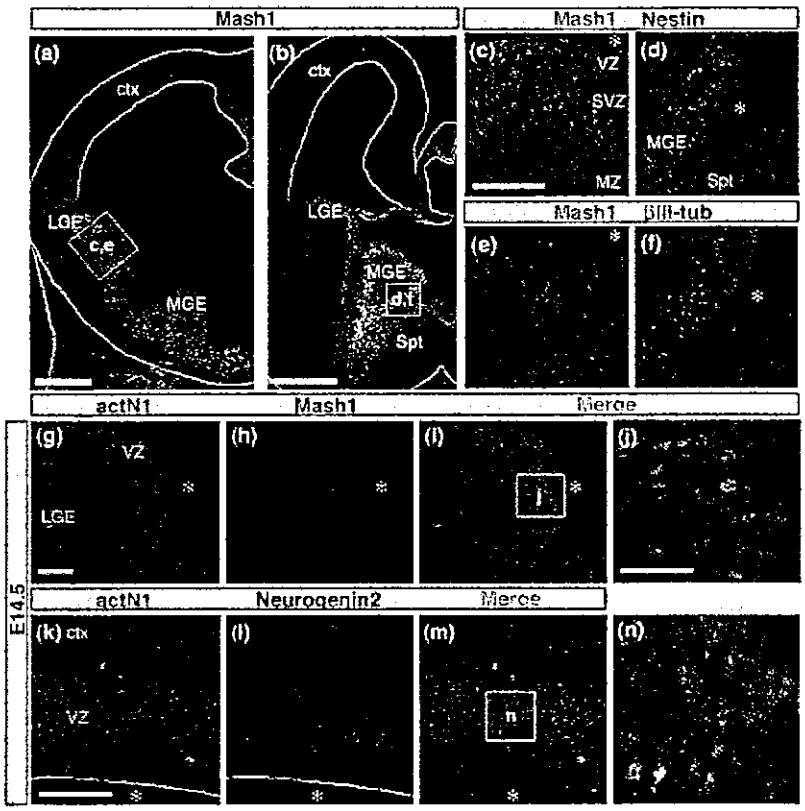

Fig. 5 Activated Notch1 and Mash1 expression patterns show no overlap. Immunostaining images of the anti-Mash1 and Ngn2 antibodies. (a–f) Mash1 was strongly expressed in the neuroepithelium of the basal telencephalic plate. White lines indicate the edge of the tissue at E11.5 (a) and E14.5 (b). Mash1-positive cells (green) were double labeled with Nestin (c, d, red) but not βIII-tubulin (e, f, red) at E11.5 and E14.5. (g–j) Activated Notch1 (green) and Mash1 (red) were expressed at high levels in the neuroepithelium, although the expression patterns were complementary at E14.5. (i) was merged image of (g,h). (j) Higher magnification views of the areas boxed in (i). (k–n) Activated Notch1 (green) and Ngn2 (red) were complementarily expressed in the neuroepithelium of the cortex at E14.5. Coronal sections: E11.5 (a,c,e) and E14.5 (b,d,f,g–n) embryos. Asterisk: lateral ventricle. Cortex (ctx), lateral ganglionic eminence (LGE), medial ganglionic eminence (MGE), septum (Spt), ventricular zone (VZ), subventricular zone (SVZ), mantle zone (MZ). Scale bars: a, 125 μm; b, 250 μm; c–f, 50 μm; g–i,k–m, 50 μm; j,n, 25 μm.

1989). At P0, the majority of cells within the VZ are identified as radial glia. At P8, the proportion of radial glia had decreased while the proportion of immature astrocytes increased. The disappearance of Nestin-positive radial glial cells from the telencephalon correlated with the appearance of GFAP-positive astrocytes (Tramontin *et al.* 2003). Radial glia are thought to give rise to GFAP-positive astrocytes. However, the intermediate cells in this transition (astrocyte precursors) have not been identified in mammalian brains because of the absence of an exclusively specific marker. We immunohistochemically investigated the transition of radial glia to astrocytes using antibodies to several molecules expressed in radial glial and/or astrocytes: BLBP, GS and GFAP. GS is known to be detectable in astrocytes and some radial glial cells (Akimoto *et al.* 1993). The temporal expression profiles of these markers showed some overlap, although the profiles were not identical, during the transition from radial glia to astrocytes. Thus, the putative astrocyte precursors could be estimated using a combination of these markers. In the present observation, we found that BLBP, but not GS, was expressed in radial glia in the VZ at E14.5 (Fig. 6a–c). GS-positive cells appeared in the radial glial cells in the germinal zone of the striatum at E17.5. Interestingly, these GS-positive cells were closely colocalized with BLBP (Fig. 6d–f), but the Mash1 and GS expression patterns did not overlap (Fig. 6g–i). Next, by combining immunostaining for activated Notch1 and astrocytic lineage markers, we found that Notch1-IR stained proliferating progenitor cells in the VZ, which also contained GS-positive cells (Fig. 6j–l). Furthermore, most of the actN1-IR was confined to the VZ in a pattern similar to that seen with GS immunostaining at E17.5 (Fig. 6m–o). At P0, GS-positive cells were found at scattered locations, apparently exhibiting radial migration, and were coexpressed with BLBP in the mantle layer (Fig. 7a–c). The GS-positive cells within the VZ, which were also actN1-IR positive, had small, round cell bodies (Fig. 7d–f); their morphologies were similar to those described previously for glial precursor cells (Levison and Goldman 1993; Levison *et al.* 1993; Zerlin *et al.* 1995). GFAP-positive cells have not yet appeared in the lateral ventricular wall at P0. These cells began to appear at P7, and by P15 GFAP staining is abundant in the lateral ventricular wall (Gates *et al.* 1995; Tramontin *et al.* 2003). In the P8 brain, a subset of putatively migrating glial cells that express GS are sparsely distributed along what are thought to be pathways toward the corpus callosum and cerebral cortex (Tramontin *et al.* 2003). GS-IR was detected in GFAP-positive differentiated astrocytes at P8 (Fig. 7g–i). Thus, GS expression is likely to have occurred in BLBP-positive radial glia and to have remained in GFAP-positive differentiated astrocytes. These results led us to suppose that the GS-positive cells may include astroglial precursor cells. In the P8 brain, a part of actN1-IR was colocalized with GFAP-IR in a region near the VZ (Fig. 7j,k). In addition, actN1-IR almost never labeled dispersed mature fibrous astrocytes expressing GFAP in the white matter (data not shown). These results suggested that Notch1 is strongly activated in the early phase of astroglial differentiation, but is down-regulated during the terminal differentiation of astrocytes.

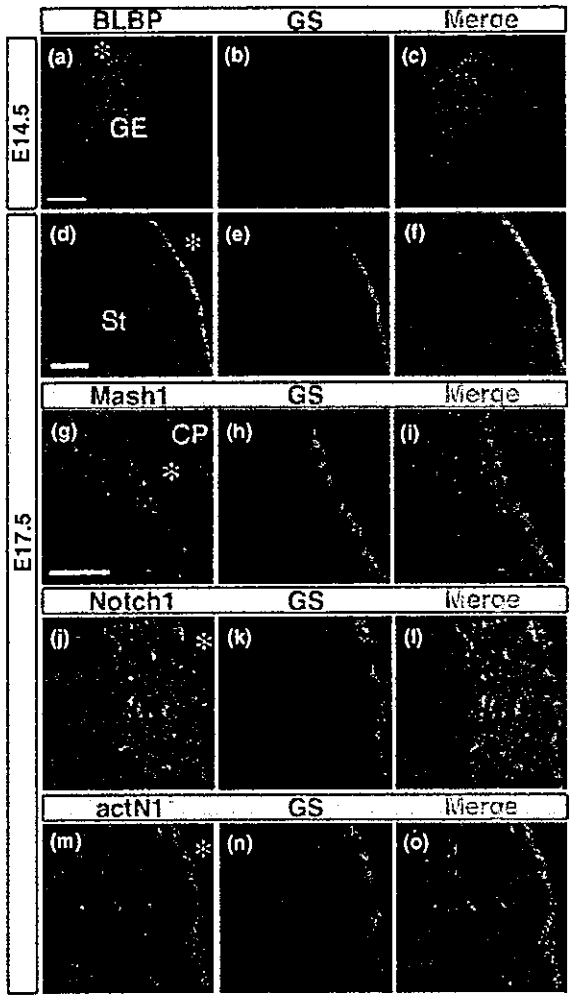

Fig. 6 Activated Notch1 is expressed in GS-positive radial glial cells. (a–c) Brain sections were immunostained with antibodies against BLBP (green) and GS (red). BLBP was expressed in the VZ of the basal forebrain, but GS expression was not observed at E14.5. (d–f) GS (red) was coexpressed with BLBP (green) in the VZ of the striatum at E17.5. (g–i) Dual labeling with Mash1-IR (green) and GS-IR (red) shows no overlapping areas. (j–l) Dual labeling of Notch1 (green) and GS (red) shows overlapping areas. (m–o) Dual labeling of activated Notch1 (green) and GS (red) shows close colocalization. Coronal sections: E14.5 (a–c) and E17.5 (d–o) embryos. Asterisk: lateral ventricle. Ganglionic eminence (GE), striatum (St), choroid plexus (CP). Scale bars: a–c,g–o, 50 μm; d–f, 100 μm.

It should be also interesting to examine the activation profile of Notch1 in the SVZ astrocytes in the adult forebrains (i.e. the adult NSCs) (Doetsch *et al.* 1999). However, we

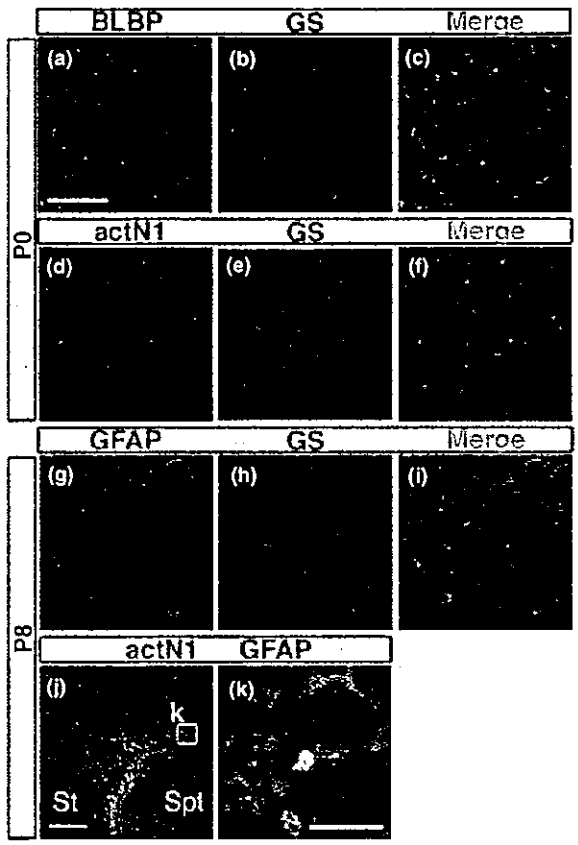

Fig. 7 Notch1 expression is retained in astrocytes. (a–c) The expression pattern of GS (red) was compared with that of BLBP (green) in the P0 forebrain at P0. BLBP and GS double-positive cells were detected in the ventrolateral area of the mantle layer. (d–f) actN1/GS-double-positive astroglial cells were sparsely distributed in the same area shown in (a–c). (g–i) Double immunofluorescence staining at P8 revealed that GS-positive cells also expressed the astrocytic marker GFAP. (j,k) Dual labeling of activated Notch1 (green) and GFAP (red) shows colocalization in the P8 brain. (k) shows higher magnification views of the boxed areas in (j).Coronal sections: P0 (a-f) and P8 (g-k) brains. Asterisk: lateral ventricle. Striatum (St), septum (Spt). Scale bars: a–j, 50 μm; k, 20 μm.

found that the actN1-immunostaing was hardly detectable in the adult forebrain SVZ (data not shown).

Discussion

Visualization of activated Notch1 *in situ*

Although Notch signaling has been reported to play important roles in development, its spatio-temporal activation pattern was unknown during CNS development. Furthermore, the ligand-dependent nuclear translocation of N1-ICD has not been detected immunohistochemically in almost of the organisms examined so far (Fehon *et al.* 1991; Lieber *et al.* 1993; Rebay *et al.* 1993), except for that identified in mouse postmigratory cortical neurons (Sestan *et al.* 1999). However, notably, even in that study, nuclear localization of N1-ICD was not detected in the proliferating precursor cells in the VZ or SVZ of embryonic forebrain (Sestan *et al.* 1999), where Notch1 activation is likely to occur (Gaiano and Fishell 2002). The low level of activated Notch1 in the nucleus is the most likely explanation for why nuclear Notch had not been detected in spite of the functional activation of Notch signaling reported in the above studies (discussed in Schroeter *et al.* 1998; Struhl and Adachi 1998).

To overcome this problem, in the present study we tried to detect endogenous Notch1 expression and its activation pattern immunohistochemically with higher sensitivity. Our present results show that anti-actN1 antibody can specifically detect the activated form of Notch1, and with higher sensitivity than the conventional anti-Notch1 antibody.

Lateral inhibition model of Notch signaling in mammalian CNS

In the present study, to characterize the cell-type specificity of the Notch1-activated cells, we examined various marker molecules expressed in developing CNS. First, we compared the activation pattern of Notch1 with that of Nestin in the embryonic brain. The results showed that at least subsets of Nestin-positive cells with radial glia-like morphology showed nuclear immunoreactivity to actN1 antibody (Fig. 4j–l). Recently, it was shown that radial glia could actually behave as multipotent NSCs that can generate neurons and glia (Kriegstein and Gotz 2003). Consistent with this, previous studies showed that misexpression of the activated form of Notch1 (N1-ICD) in the embryonic mouse brain promotes radial glial identity (Gaiano *et al.* 2000). Thus, activation of endogenous Notch1 signaling may be involved in the acquisition and/or maintenance of radial glial identity.

Next, we characterized the Notch1-activation pattern, especially in its relation to the expression of proneural bHLH gene Mash1 in the germinal zone of the GE. Neuronal precursors in this region express *Mash1*, the murine homolog of the *Drosophila achaete–scute* complex (*AS-C*) (Franco del Amo *et al.* 1993; Guillemot *et al.* 1993). Mash1-positive precursor cells in the GE might correspond mostly to neuronal precursor cells (discussed in Hartfuss *et al.* 2001). Both *Mash1* and *Notch1* mRNA were detected in similar areas during early murine CNS development (Guillemot and Joyner 1993). Interestingly, however, the Mash1-positive cell populations did not overlap with the activated Notch1-positive cells, as shown in Fig. 5. These results suggest that the activation of Notch1 normally inhibits the expression of Mash1, just as it inhibits the expression of *AS-C* in *Drosophila*. In *Drosophila*, proteins encoded by the *AS-C* genes up-regulate Delta expression in neuronal precursors (i.e. neuroblasts) (Kunisch *et al.* 1994). In addition, Notch activation during lateral inhibition results in the down-regulation of both *AS-C* and Delta expression (Lewis 1996).

In mammalian CNS, newly generated neurons up-regulate the expression of Delta as they differentiate (Casarosa *et al.* 1999). Taken together, these observations suggest that *AS-C* homologs, such as Mash1, may regulate the murine DSL genes (Ma *et al.* 1997). Given that Mash1 is required for neurogenesis in the developing mouse brain, the overlapping expression of Notch1, Delta1, and Mash1 in this region strengthens the idea that these genes participate in a common pathway (Lindsell *et al.* 1996). Thus, tracking the expression of Mash1 may also be a way to monitor the expression of Notch ligands. Mash1-positive cells, which probably express higher amount of Notch ligands, and actN1-positive cells, in which the Notch signaling is activated, were close neighbors, although there was never any overlap in the immunostaining for these molecules (Fig. 5). This result indicates that lateral inhibition might function in these cells.

The Mash1-positive cells in the embryonic GE are known to be precursors for GABAnergic neurons (Kriegstein and Gotz 2003; Malatesta *et al.* 2003; Ross *et al.* 2003). Thus, an attractive model would be that the differential activation of Notch1 in the GE, possibly through lateral inhibition, results in the divergence of two different precursors: precursors for GABAergic neurons (Mash1-positive and actN1-negative) and radial glia committed to an astroglial fate (Mash1-negative and actN1-positive). In addition, Ngn2 is predicted to have the same function as Mash1 in the embryonic cortex, based on the complementary expression of Ngn2 and actN1.

Notch1 activation in glial lineage cells during perinatal CNS development

Recently, it is suggested that Notch1 signaling is Involved in the maintenance of progenitor cells (Artavanis-Tsakonas *et al.* 1999), including progenitors destined to a neuronal fate (Nakamura *et al.* 2000), in an undifferentiated state as well as the promotion of glial fates in mammalian CNS development (Tanigaki *et al.* 2001). The temporal pattern of Notch1 expression differed between neuronal and glial cells; the neuronal expression of Notch1 diminished after the progenitor cells differentiated into neurons (Fig. 4h). Although there has been some debate (Wang and Barres 2000; Gaiano and Fishell 2002; Sun *et al.* 2003), the role of Notch signaling is not completely understood in glial development.

A previous study, in which the activated form of Notch1 was overexpressed in rat adult hippocampus-derived multipotent progenitors, suggests an instructive role for Notch signaling to promote astrocytic fate (Tanigaki *et al.* 2001). In this gain-of-function study *in vitro*, they showed that transient activation of Notch1 (4-hydroxytamoxifen-induced nuclear transport of N1-ICD that had been fused to the estrogen receptor) is sufficient to promote astrocytic fate. To clarify the *in vivo* significance of this finding, it was important to characterize the temporal activation of Notch1 signaling during glial development *in vivo*.

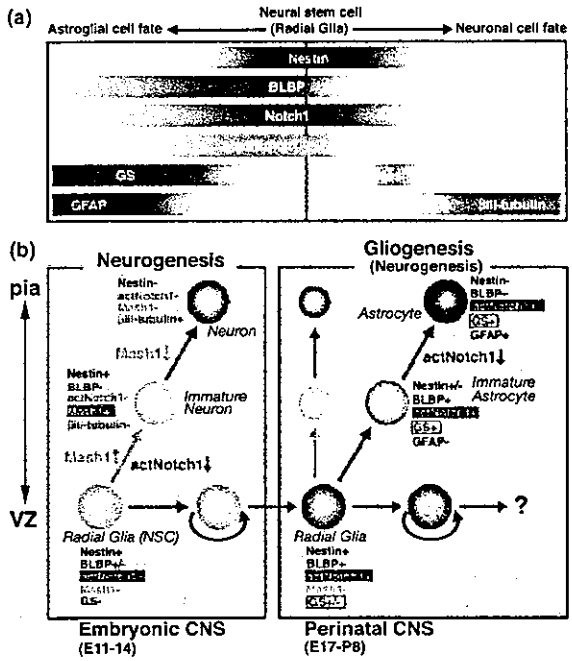

Fig. 8 Model for the expression and function of Notch1 signaling during CNS development. (a) Sequential expression patterns of activated Notch1, Mash1, and several lineage markers during the histogenesis of the CNS. The expressions of activated Notch1, Notch1, Mash1, Nestin, BLBP, GS, GFAP, and βIII-tubulin are initiated in the order given, as development proceeds from neurogenesis to gliogenesis and to neural cell maturation. This scheme includes the results shown in the Table, where mutually overlapping and/or exclusive expression patterns among these antigens are described. (b) Schematic representation of the activation of Notch signaling during embryonic and perinatal CNS development.

In the present study, the glial expression of Notch1 continued even after glial cells became positive for GFAP (Fig. 7k). However, we found that activation of Notch1 was not continuous (data not shown). At least two stages can be distinguished in glial differentiation, as described here (Fig. 8b, right). In the first stage, immature glia express little or none of the glial marker GFAP, but they express significant levels of GS. The immature glia also express activated Notch1 at a high level. In the second stage of glial differentiation, the maturing glia expressed GFAP and was shown little or no Notch1 activation (Figs 7 and 8b). The molecular mechanism responsible for the transient activation of Notch1, resulting in the astrocytic differentiation of neural stem/progenitor cells, remains to be elucidated. However, a recent study has indicated that the corepressor NcoR inhibits the astrocytic differentiation of neural stem/progenitor cells and represses the transcription of the *GFAP* gene by physically interacting with a DNA-binding protein, CSL, that binds directly to the repressor region of the *GFAP* promoter (Hermanson *et al.* 2002; Ge *et al.* 2002). On the

other hand, upon Notch1 activation, N1-ICD translocates into the nucleus to form a complex with CSL (Kato *et al.* 1997), thereby changing CSL from a transcriptional repressor into an activator and stimulating the transcription of its target genes (Beatus *et al.* 2001). Thus, an attractive model would be that the transient activation of Notch1 might de-repress *GFAP* transcription by recruiting N1-ICD into the CSL complex through the exclusion of NcoR from the CSL complex bound to the *GFAP* promoter. Consistent with this theory, the removal of NCoR is indeed sufficient to induce *GFAP* expression *in vivo* and *in vitro* (Hermanson *et al.* 2002). However, whether the transcriptional activator complex, including N1-ICD and CSL, is maintained on the *GFAP* promoter during the maturation of astrocytes must be determined by detailed molecular studies. Future studies concomitantly characterizing the functions of the above-mentioned transcriptional regulators and *in situ* detection of the activated form of Notch1 described in the present study would reveal the significance of the context-dependent actions of Notch signaling.

Acknowledgements

We thank Tetsuo Sudo for rabbit anti-Hes1 antibody, Nathaniel Heintz for rabbit anti-BLBP antibody and David J. Anderson for mouse anti-Neurogenin2. We are grateful to Drs Yukiko Gotoh, Ola Hermanson, Takuya Shimazaki and Shin-ichi Sakakibara for critical comments to this manuscript. This work was supported by grants to HO from the Japanese Ministry of Education, Culture, Sports, Science and Technology, from Japan Science and Technology Agency (CREST), and by a grant-in-aid from the 21th century COE program of the Ministry of Education, Science and Culture to Keio University.

References

Akimoto J., Itoh H., Miwa T. and Ikeda K. (1993) Immunohistochemical study of glutamine synthetase expression in early glial development. *Brain Res. Dev. Brain Res.* **72**, 9–14.

Alvarez-Buylla A., Garcia-Verdugo J. M. and Tramontin A. D. (2001) A unified hypothesis on the lineage of neural stem cells. *Nat. Rev. Neurosci.* **2**, 287–293.

Anderson D. J. (2001) Stem cells and pattern formation in the nervous system: the possible versus the actual. *Neuron* **30**, 19–35.

Artavanis-Tsakonas S., Rand M. D. and Lake R. J. (1999) Notch signaling: cell fate control and signal integration in development. *Science* **284**, 770–776.

Beatus P. and Lendahl U. (1998) Notch and neurogenesis. *J. Neurosci. Res.* **54**, 125–136.

Beatus P., Lundkvist J., Oberg C., Pedersen K. and Lendahl U. (2001) The origin of the ankyrin repeat region in Notch intracellular domains is critical for regulation of HES promoter activity. *Mech. Dev.* **104**, 3–20.

Casarosa S., Fode C. and Guillemot F. (1999) Mash1 regulates neurogenesis in the ventral telencephalon. *Development* **126**, 525–534.

Chambers C. B., Peng Y., Nguyen H., Gaiano N., Fishell G. and Nye J. S. (2001) Spatiotemporal selectivity of response to Notch1 signals in mammalian forebrain precursors. *Development* **128**, 689–702.

Doetsch F., Caille I., Lim D. A., Garcia-Verdugo J. M. and Alvarez-Buylla A. (1999) Subventricular zone astrocytes are neural stem cells in the adult mammalian brain. *Cell* **97**, 703–716.

Fehon R. G., Johansen K., Rebay I. and Artavanis-Tsakonas S. (1991) Complex cellular and subcellular regulation of notch expression during embryonic and imaginal development of Drosophila: implications for notch function. *J. Cell Biol.* **113**, 657–669.

Feng L. and Heintz N. (1995) Differentiating neurons activate transcription of the brain lipid-binding protein gene in radial glia through a novel regulatory element. *Development* **121**, 1719–1730.

Feng L., Hatten M. E. and Heintz N. (1994) Brain lipid-binding protein (BLBP): a novel signaling system in the developing mammalian CNS. *Neuron* **12**, 895–908.

Fode C., Ma Q., Casarosa S., Ang S. L., Anderson D. J. and Guillemot F. (2000) A role for neural determination genes in specifying the dorsoventral identity of telencephalic neurons. *Genes Dev.* **14**: 67–80.

Franco del Amo F., Gendron-Maguire M., Swiatek P. J. and Gridley T. (1993) Cloning, sequencing and expression of the mouse mammalian achaete-scute homolog 1 (MASH1). *Biochim. Biophys. Acta* **1171**, 323–327.

Gaiano N. and Fishell G. (2000) Notch1 signaling promotes the formation of bFGF-responsive neurospheres derived from embryonic mouse telencephalon. *Society of Neuroscience 31st Annual Meeting (Abstract)* **26**, 1347.

Gaiano N. and Fishell G. (2002) The role of notch in promoting glial and neural stem cell fates. *Annu. Rev. Neurosci.* **25**, 471–490.

Gaiano N., Nye J. S. and Fishell G. (2000) Radial glial identity is promoted by Notch1 signaling in the murine forebrain. *Neuron* **26**, 395–404.

Gates M. A., Thomas L. B., Howard E. M., Laywell E. D., Sajin B., Faissner A., Gotz B., Silver J. and Steindler D. A. (1995) Cell and molecular analysis of the developing and adult mouse subventricular zone of the cerebral hemispheres. *J. Comp. Neurol.* **361**, 249–266.

Ge W., Martinowich K., Wu X., He F., Miyamoto A., Fan G., Weinmaster G. and Sun Y. E. (2002) Notch signaling promotes astrogliogenesis via direct CSL-mediated glial gene activation. *J. Neurosci. Res.* **69**, 848–860.

Guillemot F. and Joyner A. L. (1993) Dynamic expression of the murine Achaete-Scute homologue Mash-1 in the developing nervous system. *Mech. Dev.* **42**, 171–185.

Guillemot F., Lo L. C., Johnson J. E., Auerbach A., Anderson D. J. and Joyner A. L. (1993) Mammalian achaete-scute homolog 1 is required for the early development of olfactory and autonomic neurons. *Cell* **75**, 463–476.

Hartfuss E., Galli R., Heins N. and Gotz M. (2001) Characterization of CNS precursor subtypes and radial glia. *Dev. Biol.* **229**, 15–30.

Hermanson O., Jepsen K. and Rosenfeld M. G. (2002) N-CoR controls differentiation of neural stem cells into astrocytes. *Nature* **419**, 934–939.

Hitoshi S., Alexson T., Tropepe V., Donoviel D., Elia A. J., Nye J. S., Conlon R. A., Mak T. W., Bernstein A. and van der Kooy D. (2002) Notch pathway molecules are essential for the maintenance, but not the generation, of mammalian neural stem cells. *Genes Dev.* **16**, 846–858.

Hockfield S. and McKay R. D. (1985) Identification of major cell classes in the developing mammalian nervous system. *J. Neurosci.* **5**, 3310–3328.

Ishibashi M., Ang S. L., Shiota K., Nakanishi S., Kageyama R. and Guillemot F. (1995) Targeted disruption of mammalian hairy and Enhancer of split homolog-1 (HES-1) leads to up-regulation of neural helix-loop-helix factors, premature neurogenesis, and severe neural tube defects. *Genes Dev.* **9**, 3136–3148.

Ito T, Udaka N, Yazawa T, Okudela K, Hayashi H, Sudo T, Guillemot F, Kageyama R. and Kitamura H (2000) Basic helix-loop-helix transcription factors regulate the neuroendocrine differentiation of fetal mouse pulmonary epithelium. *Development* **127**, 3913–3921.

Jarriault S., Brou C., Logeat F., Schroeter E. H., Kopan R. and Israel A. (1995) Signalling downstream of activated mammalian Notch. *Nature* **377**, 355–358.

Jarriault S., Le Bail O., Hirsinger E., Pourquie O., Logeat F., Strong C. F., Brou C., Seidah N. G. and Isra 1 A. (1998) Delta-1 activation of notch-1 signaling results in HES-1 transactivation. *Mol. Cell Biol.* **18**, 7423–7431.

Kageyama R. and Nakanishi S. (1997) Helix-loop-helix factors in growth and differentiation of the vertebrate nervous system. *Curr. Opin. Genet. Dev.* **7**, 659–665.

Kato H., Taniguchi Y., Kurooka H., Minoguchi S., Sakai T., Nomura-Okazaki S., Tamura K. and Honjo T. (1997) Involvement of RBP-J in biological functions of mouse Notch1 and its derivatives. *Development* **124**, 4133–4141.

Kopan R., Schroeter E. H., Weintraub H. and Nye J. S. (1996) Signal transduction by activated mNotch: importance of proteolytic processing and its regulation by the extracellular domain. *Proc. Natl Acad. Sci. USA* **93**, 1683–1688.

Kriegstein A. R. and Gotz M. (2003) Radial glia diversity: a matter of cell fate. *Glia* **43**, 37–43.

Kunisch M., Haenlin M. and Campos-Ortega J. A. (1994) Lateral inhibition mediated by the Drosophila neurogenic gene delta is enhanced by proneural proteins. *Proc. Natl Acad. Sci. USA* **91**, 10139–10143.

Kurtz A., Zimmer A., Schnutgen F., Bruning G., Spener F. and Muller T. (1994) The expression pattern of a novel gene encoding brain-fatty acid binding protein correlates with neuronal and glial cell development. *Development* **120**, 2637–2649.

Lendahl U., Zimmerman L. B. and McKay R. D. (1990) CNS stem cells express a new class of intermediate filament protein. *Cell* **60**, 585–595.

Levison S. W., Chuang C., Abramson B. J. and Goldman J. E. (1993) The migrational patterns and developmental fates of glial precursors in the rat subventricular zone are temporally regulated. *Development* **119**, 611–622.

Levison S. W. and Goldman J. E. (1993) Both oligodendrocytes and astrocytes develop from progenitors in the subventricular zone of postnatal rat forebrain. *Neuron* **10**, 201–212.

Lewis J. (1996) Neurogenic genes and vertebrate neurogenesis. *Curr. Opin. Neurobiol.* **6**, 3–10.

Li Y. M., Xu M., Lai M. T., Huang Q. *et al.* (2000) Photoactivated gamma-secretase inhibitors directed to the active site covalently label presenilin 1. *Nature* **405**, 689–694.

Lieber T., Kidd S., Alcamo E., Corbin V. and Young M. W. (1993) Antineurogenic phenotypes induced by truncated Notch proteins indicate a role in signal transduction and may point to a novel function for Notch in nuclei. *Genes Dev.* **7**, 1949–1965.

Lindsell C. E., Boulter J., diSibio G., Gossler A. and Weinmaster G. (1996) Expression patterns of Jagged, Delta1, Notch1, Notch2, and Notch3 genes identify ligand-receptor pairs that may function in neural development. *Mol. Cell. Neurosci.* **8**, 14–27.

Lo L., Dormand E., Greenwood A. and Anderson D. J. (2002) Comparison of the generic neuronal differentiation and neuron subtype specification functions of mammalian achaete-scute and atonal homologs in cultured neural progenitor cells. *Development* **129**, 1553–1567.

Ma Q., Sommer L., Cserjesi P. and Anderson D. J. (1997) Mash1 and neurogenin1 expression patterns define complementary domains of neuroepithelium in the developing CNS and are correlated with regions expressing notch ligands. *J. Neurosci.* **17**, 3644–3652.

Malatesta P., Hack M. A., Hartfuss E., Kettenmann H., Klinkert W., Kirchhoff F. and Gotz M. (2003) Neuronal or glial progeny: regional differences in radial glia fate. *Neuron* **37**, 751–764.

Miyata T., Kawaguchi A., Okano H. and Ogawa M. (2001) Asymmetric inheritance of radial glial fibers by cortical neurons. *Neuron* **31**, 727–741.

Nakamura Y., Sakakibara S., Miyata T., Ogawa M., Shimazaki T., Weiss S., Kageyama R. and Okano H. (2000) The bHLH gene hes1 as a repressor of the neuronal commitment of CNS stem cells. *J. Neurosci.* **20**, 283–293.

Nieto M., Schuurmans C., Britz O. and Guillemot F. (2001) Neural bHLH genes control the neuronal versus glial fate decision in cortical progenitors. *Neuron* **29**, 401–413.

Nye J. S., Kopan R. and Axel R. (1994) An activated Notch suppresses neurogenesis and myogenesis but not gliogenesis in mammalian cells. *Development* **120**, 2421–2430.

Okano H. (2002) Stem cell biology of the central nervous system. *J. Neurosci. Res.* **69**, 698–707.

de la Pompa J. L., Wakeham A., Correia K. M. *et al.* (1997) Conservation of the Notch signalling pathway in mammalian neurogenesis. *Development* **124**, 1139–1148.

Qian X., Shen Q., Goderie S. K., He W., Capela A., Davis A. A. and Temple S. (2000) Timing of CNS cell generation: a programmed sequence of neuron and glial cell production from isolated murine cortical stem cells. *Neuron* **28**, 69–80.

Rakic P. (2003) Elusive radial glial cells: historical and evolutionary perspective. *Glia* **43**, 19–32.

Rebay I., Fehon R. G. and Artavanis-Tsakonas S. (1993) Specific truncations of *Drosophila* Notch define dominant activated and dominant negative forms of the receptor. *Cell* **74**, 319–329.

Ross S. E., Greenberg M. E. and Stiles C. D. (2003) Basic helix-loop-helix factors in cortical development. *Neuron* **39**, 13–25.

Saito T. and Nakatsuji N. (2001) Efficient gene transfer into the embryonic mouse brain using *in vivo* electroporation. *Dev. Biol.* **240**, 237–246.

Schmechel D. E. and Rakic P. (1979) Arrested proliferation of radial glial cells during midgestation in rhesus monkey. *Nature* **277**, 303–305.

Schroeter E. H., Kisslinger J. A. and Kopan R. (1998) Notch-1 signalling requires ligand-induced proteolytic release of intracellular domain. *Nature* **393**, 382–386.

Selkoe D. and Kopan R. (2003) Notch and presenilin: regulated intramembrane proteolysis links development and degeneration. *Annu. Rev. Neurosci.* **26**, 565–597.

Sestan N., Artavanis-Tsakonas S. and Rakic P. (1999) Contact-dependent inhibition of cortical neurite growth mediated by notch signaling. *Science* **286**, 741–746.

Struhl G. and Adachi A. (1998) Nuclear access and action of notch *in vivo*. *Cell* **93**, 649–660.

Sun Y., Nadal-Vicens M., Misono S., Lin M. Z., Zubiaga A., Hua X., Fan G. and Greenberg M. E. (2001) Neurogenin promotes neurogenesis and inhibits glial differentiation by independent mechanisms. *Cell* **104**, 365–376.

Sun Y. E., Martinowich K. and Ge W. (2003) Making and repairing the mammalian brain – signaling toward neurogenesis and gliogenesis. *Semin. Cell Dev. Biol.* **14**, 161–168.

Tanigaki K., Nogaki F., Takahashi J., Tashiro K., Kurooka H. and Honjo T. (2001) Notch1 and Notch3 instructively restrict bFGF-responsive multipotent neural progenitor cells to an astroglial fate. *Neuron* **29**, 45–55.

Torii M., Matsuzaki F., Osumi N., Kaibuchi K., Nakamura S., Casarosa S., Guillemot F. and Nakafuku M. (1999) Transcription factors Mash-1 and Prox-1 delineate early steps in differentiation of neural stem cells

in the developing central nervous system. *Development* **126**, 443–456.

Tramontin A. D., Garcia-Verdugo J. M., Lim D. A. and Alvarez-Buylla A. (2003) Postnatal development of radial glia and the ventricular zone (VZ): a continuum of the neural stem cell compartment. *Cereb. Cortex* **13**, 580–587.

Voigt T. (1989) Development of glial cells in the cerebral wall of ferrets: direct tracing of their transformation from radial glia into astrocytes. *J. Comp. Neurol.* **289**, 74–88.

Wang S. and Barres B. A. (2000) Up a notch: instructing gliogenesis. *Neuron* **27**, 197–200.

Weinmaster G., Roberts V. J. and Lemke G. (1991) A homolog of Drosophila Notch expressed during mammalian development. *Development* **113**, 199–205.

Yamamoto N., Yamamoto S., Inagaki F. *et al.* (2001) Role of Deltex-1 as a transcriptional regulator downstream of the Notch receptor. *J. Biol. Chem.* **276**, 45031–45040.

Zerlin M., Levison S. W. and Goldman J. E. (1995) Early patterns of migration, morphogenesis, and intermediate filament expression of subventricular zone cells in the postnatal rat forebrain. *J. Neurosci.* **15**, 7238–7249.

Human Molecular Genetics, 2005, Vol. 14, No. 6 1–11
doi:10.1093/hmg/ddi069
Advance Access published on xxx

The *Pax6* isoform bearing an alternative spliced exon promotes the development of the neural retinal structure

Noriyuki Azuma[1,2,*], Keiko Tadokoro[2], Astuko Asaka[2], Masao Yamada[2], Yuki Yamaguchi[3], Hiroshi Handa[3], Satsuki Matsushima[4], Takashi Watanabe[4], Shinichi Kohsaka[5], Yasuyuki Kida[6], Tomoki Shiraishi[6], Toshihiko Ogura[6], Kenji Shimamura[7] and Masato Nakafuku[7]

[1]Department of Ophthalmology, National Center for Child Health and Development, Tokyo 157-8535, Japan, [2]Department of Genetics, National Research Institute for Child Health and Development, Tokyo 154-8567, Japan, [3]Department of Biological Information, Tokyo Institute of Technology, Graduate School of Bioscience and Biotechnology, Yokohama, 226-8501, Japan, [4]Department of Clinical Pathology, Kyorin University School of Medicine, Tokyo 181-8611, Japan, [5]Department of Neurochemistry, National Institute of Neuroscience, Tokyo, 187-8502, Japan, [6]Department of Developmental Neurobiology, Institute of Development, Aging and Cancer, Sendai 980-8575, Japan and [7]Department of Neuroscience, University of Tokyo Graduate School of Medicine, Tokyo 113-0033, Japan

Received November 28, 2004; Accepted January 18, 2005

The vertebrate retina has an area where visual cells are closely packed for proper vision that is known as a fovea, an area centralis or a visual streak. The molecular mechanism that regulates the formation of these structures and visual cell gradients is unknown. The transcription factor Pax6 is a master regulator of eye development. A Pax6 isoform that contains an exon 5a-encoded 14 amino acid insertion in its paired domain, Pax6(+5a), has different DNA-binding properties compared with the Pax6(−5a) isoform. Little is known about the functional significance of Pax6(+5a). Here, we show that Pax6(+5a) is expressed especially in the retinal portion where visual cells accumulate during eye development and, when overexpressed, induces a remarkable well-differentiated retina-like structure. Pax6(+5a) proteins that bear point mutations that are found in patients with foveal hypoplasia are unable to induce these ectopic retina-like structures. We propose that Pax6(+5a) induces a developmental cascade in the prospective fovea, area centralis or visual streak region that leads to the formation of a retinal architecture bearing densely packed visual cells.

INTRODUCTION

Most vertebrates have a region of the retina where cone photoreceptors, bipolar cells and ganglion cells accumulate and specialize, which contributes to better vision (1–3). This region comes in two general forms, namely, a visual streak and an area centralis. Animals that are nocturnal or have relatively poor vision bear a visual streak, where the photoreceptors, bipolar cells and ganglion cells congregate and become specialized along a horizontal line of the eye fundus. In contrast, animals that have relatively good vision bear the area centralis, which is a circular spot in the retina. The image of an object becomes centered on this region. A specialized form of the area centralis is the fovea, which helps many reptiles and birds, and most primates achieve greater visual sensitivity. The fovea is an area in which cone photoreceptors are highly concentrated and the inner retina is thinned. Human patients lacking the fovea have a poor visual acuity of 0.1–0.3, even with lens correction (4,5). Thus, the fovea is an essential architectural feature that is required for our sharp visual acuity.

In most vertebrates that have a fovea or an area centralis, the retinal cells first accumulate, differentiate and form synaptic connections at the prospective fovea or area centralis

*To whom correspondence should be addressed at: Department of Ophthalmology, National Center for Child Health and Development, 2-10-1 Okura, Setagaya-ku, Tokyo 157-8535, Japan. Tel: +81 334160181; Fax: +81 334162222; Email: azuma-n@ncchd.go.jp

region during the very early stages of eye development, corresponding to the time when ganglion cells appear in the retina. The differentiation of the retinal cells then progresses from the centre to the periphery, which results in a gradient of visual sensitivity (2,3). The molecular mechanisms that regulate the formation of these specific retinal structures are not well elucidated, although previous studies have explored mechanism and genes involved in differentiation of the retinal area (6–8).

Recently, patients with foveal hypoplasia were found to bear mutations in the *PAX6* gene (4,5). The *Pax6* gene encodes a transcription factor and plays important roles in eye morphogenesis in both vertebrates and invertebrates (9–12). This gene has been reported to induce ectopic eye formation in *Drosophila melanogaster* (13) and *Xenopus* larvae (14), and is known as a master control gene in eye formation (9–11). Pax6 is expressed in various eye tissues. In the neural retina, Pax6 is expressed widely in multipotent progenitor cells at early stages and to a lesser extent in ganglion, horizontal and amacrine cells at late stages (15–17). The *Pax6* gene produces two isoforms by alternative splicing, namely, Pax6(−5a) and Pax6(+5a). Pax6(+5a) differs from Pax6(−5a) by the presence of an exon 5a-encoded 14 amino acid insertion in its paired-type DNA-binding domain (paired domain, or PD) (18,19). Pax6(−5a) and Pax6(+5a) show distinct DNA-binding properties (20) and their distinct consensus binding sequences have been determined. These are termed P6CON and 5aCON, respectively (21). Mutational analyses have shown that the N-terminal subdomain (NTS) and the C-terminal subdomain (CTS) of the Pax6 PD are respectively responsible for the DNA-binding abilities of Pax6(−5a) and Pax6(+5a) and their transactivation activity (20,22). Pax6(−5a) binds to a promoter element of the *ζ-crystallin* gene at a site that is highly similar to P6CON (23), while target genes of Pax6(+5a) that bear 5aCON-like sequences are yet to be identified.

Many mutations in the *PAX6* gene have been identified in human patients with foveal hypoplasia (4,5,24–27). In most classical aniridia patients, caused by haploinsufficiency of PAX6 due to its deletion or the presence of a nonsense mutation, all other eye tissues apart from the iris, including the cornea, lens, fovea and optic nerve, are also affected. In contrast, missense mutations in the *PAX6* gene cause more specific eye anomalies (4,5,25–27), probably because Pax6 has multiple functional domains and that missense mutations in this gene disturb one or only a few of these domains. Previously, we reported two PAX6 missense mutations, R128C in the CTS of the PD and V54D in exon 5a, in Japanese patients with foveal hypoplasia (4,5). An R128C mutation was again identified in an independent European patient with the same phenotype (26). These findings suggest that the CTS and exon 5a, which are two elements that are thought to be important for the function of the Pax6(+5a) isoform, may be involved in the formation of the fovea. We investigated expression pattern of Pax6(+5a) in the developing retina and effect of the isoform in retinal development by gain-of-function experiments, and here present evidence that Pax6(+5a) contributes to promote the formation of the retinal structure.

RESULTS

Pax6(+5a) is abundantly expressed in the retinal portion where visual cells accumulate

We first examined the regional expression of the Pax6 isoforms by subjecting sections of a neonatal marmoset eye (which has a fovea) to immunohistochemical staining with two different antibodies that can distinguish between the two Pax6 isoforms. One of these antibodies, which is denoted as anti-Pax6, was raised against amino acids 1–223 including those encoded by exon 5a. This antibody reacts with both Pax6(−5a) and Pax6 (+5a), as reported previously (16,17). For this study, we raised another antibody against a synthetic peptide consisting of the 14 amino acid residues that are encoded by exon 5a (anti-exon 5a). Western blotting of proteins prepared from cultured mouse embryonic carcinoma P19 cells that had been transfected with constructs expressing Pax6(−5a) or Pax6(+5a), and of marmoset tissues expressing both isoforms demonstrated the specificity of these antibodies (Fig. 1A). On the marmoset sections, anti-Pax6 visualized three layers, namely, the ganglion cell layer and the inner and outer edges of the inner nuclear layer of the retina. The foveal region was heavily stained, and both the nasal and temporal nasal sides were also stained (Fig. 1C, middle panels). This indicates the wide distribution of Pax6 proteins throughout the entire retina. In contrast, the anti-exon 5a staining pattern suggested that the Pax6(+5a) protein localizes to a restricted retinal area between the optic nerve head and the fovea (Fig. 1C b and c). This was clear when the staining in the nasal and foveal sides of the optic nerve head was compared. The staining was identified scarcely in the nasal side but obviously in the foveal side (Fig. 1C b). From these observations, we conclude that the Pax6(+5a) isoform is expressed especially in the restricted retinal portion where the densely packed visual cells reside.

Reflecting evolutionary conservation of the amino acid sequence encoded by exon 5a, the anti-exon 5a antibody reacts with chicken Pax6(+5a) as well, albeit weakly. In the chicken retina of Hamburger–Hamilton (HH) stage 45, the Pax6(+5a) protein appears to localize in a restricted retinal area of the visual streak, whereas the Pax6(−5a) protein distributes throughout the entire retina (Fig. 2A). To compare the expression levels of the two isoforms, we next performed semi-quantitative RT–PCR analysis using dissected retinal tissues of chick embryos at HH stages 12–45. The isolated RNAs were subjected to RT–PCR analysis using specific primers that flank exon 5a and can distinguish between the two isoforms *Pax6(+5a)* and *Pax6(−5a)*. At an early developmental stage (HH stage12), when the optic vesicle is formed and multipotent progenitor cells still exist in the neural retina, the two isoforms were expressed in both the central nervous system (CNS) and the eye primordium but the *Pax6(−5a)* isoform predominated (Fig. 2B). At HH stage 20, Pax6(−5a) was still the major transcript. At this stage, the formation of the eye is proceeding and lens formation is evident. During HH stages 24–30, the ganglion cells in the retina differentiate. The level of *Pax6(−5a)* expression seems to decrease transiently at HH stage 24 and increase at HH stage 30. Interestingly, the level of *Pax6(+5a)* expression gradually increased during this period

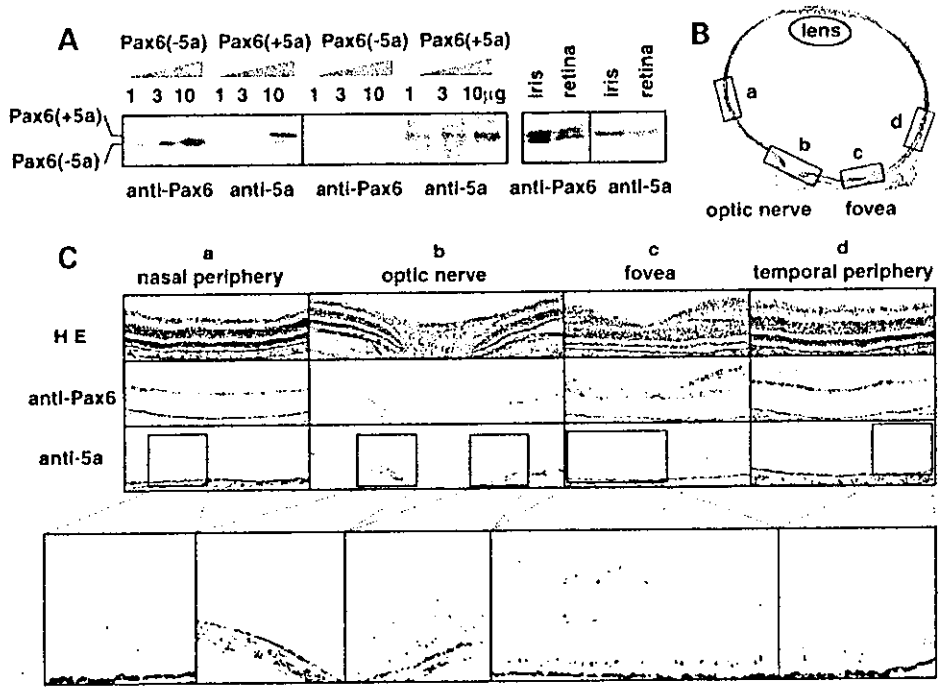

Figure 1. Histochemical analysis of the expression of the two Pax6 isoforms in the neonatal marmoset eye. (**A**) Western blotting analysis confirming the specificity of the two antibodies that were used. P19 cells (10^5 cells) were transfected with either the Pax6(−5a) or Pax6(+5a) expression construct and nuclear protein fractions obtained 24 h post-transfection were analyzed. Anti-Pax6 recognized the exogenously expressed Pax6(−5a) and Pax6(+5a) proteins as well as endogenous Pax6(−5a) protein, whereas anti-exon 5a recognized Pax6(+5a) but not Pax6(−5a). Western blotting analysis of nuclear fraction proteins obtained from the iris and retina tissues of the neonatal marmoset (*Callithrix jacchus*) also showed that anti-Pax6 recognized both native Pax6(−5a) and Pax6(+5a) proteins, whereas anti-exon 5a recognized Pax6(+5a) but not Pax6(−5a). (**B**) View of a horizontal section of the eye of a neonatal marmoset stained with HE. (**C**) Magnified fields of the eye stained with HE, anti-Pax6 or anti-exon 5a (bar scale 100 μm). Further enlarged images are shown below. a, nasal peripheral area; b, optic nerve head area; c, fovea area; d, temporal peripheral area. The staining for anti-exon 5a localizes around the fovea area, whereas that for anti-Pax6 is detected throughout the entire retina. The result shown is representative of three independent experiments using four marmoset eyes.

in all ocular tissues such as the cornea, lens and retina. Increased expression of *Pax6(+5a)* was also evident in the retina in later stages (HH stages 36–45), when all photoreceptors, horizontal and amacrine cells differentiate. Although the eyes of domestic birds lack the fovea, they possess a distinct visual streak in the posterior portion of the retina (1,2). Expression of *Pax6(+5a)* became particularly intense in this posterior portion. At HH stage 36, the expression of *Pax6(+5a)* exceeded that of *Pax6(−5a)* in the posterior retina. These observations indicate that expression of the two Pax6 isoforms are differentially regulated during retinal development, with Pax6(+5a) expression increasing only in a specified region, whereas Pax6(−5a) expression being throughout the retina.

In *ovo* misexpression of *Pax6(+5a)* gene markedly expands the retinal layer and promotes the growth and differentiation of retinal cells into visual cells

Next, we investigated the roles the two Pax6 isoforms play in the formation of the eye architecture by *in ovo* electroporation (28). Thus, an expression construct for either Pax6(+5a) or Pax6(−5a) was electroporated into the developing retina of HH stages 16–30 chick embryos, together with an expression construct of green fluorescence protein (GFP) (29) to monitor the expression of the transgenes. Expression plasmids [pCAGGS-PAX6(−5a) and pCAGGS-PAX6(+5a)] carry the entire human *PAX6* coding region with or without exon 5a under the control of a cytomegalovirus enhancer and chicken β-actin promoter, as described previously (5,22). Embryos that had been electroporated were harvested at various stages and analyzed. Retinal formation was scarcely affected when either isoform was transduced after HH stage 30 (data not shown). However, marked changes were observed when either isoform was transduced at HH stages 16–24, when the formation of the optic cup was completed. Six to twelve hours after electroporation of Pax6(−5a) and GFP (HH stage 18), the electroporated region, confirmed by staining with anti-Pax6 and anti-GFP antibodies, was found to proliferate excessively, as evidenced by intense staining with anti-5-bromo-2′-deoxyuridine (BrdU) antibody (Fig. 3). The promotion of retinal cell proliferation occurred similarly up to this stage regardless of the Pax6 isoforms overexpressed (data not shown). Electroporation of the empty vector alone, the pCAGGS-GFP or both constructs did not induce any change.

At later stages, a significant difference in the effect of the two Pax6 isoforms was observed. When Pax6(−5a) was misexpressed, 3–7 days after the electroporation (HH stages 28–35), 47% ($n = 198$) of the eyes were larger than the untreated

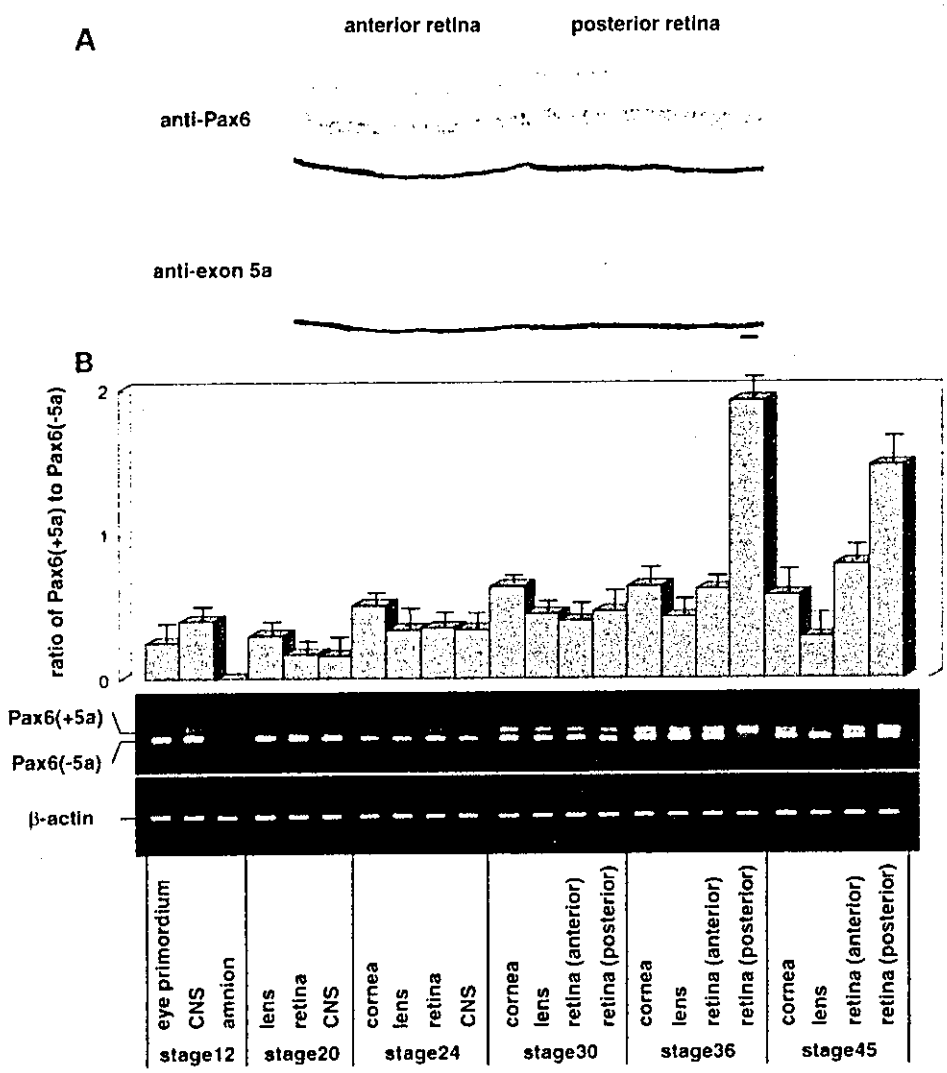

Figure 2. (A) Horizontal sections of the chick eye at HH stage 45 stained with anti-Pax6 or anti-exon 5a antibody (bar scale 20 μm). The Pax6(+5a) protein appears to localize in the posterior retina containing the visual streak, whereas the Pax6(−5a) protein distributes throughout the entire retina. (B) Semi-quantitative RT–PCR analysis of the expression of the two *Pax6* isoforms in developing chick embryos. As the eye became big enough to be dissected at later stages, *Pax6* expression could be examined in particular parts of the eye structure. The indicated PCR fragments were judged to represent one or the other *Pax6* isoform by their sizes. This was confirmed by sequencing. In the posterior retina, tissues were excised from the visual streak region. Amnion tissues were used as a negative control for *Pax6* expression and *β-actin* represents the amounts of RNA in each lane. The bar graph is shown as mean ± SD ($n = 3$) of expression ratio of Pax6(+5a) to Pax6(−5a). The photograph of RT–PCR analysis under the bar graph is representative of three independent experiments.

control eyes (Fig. 4A). Several isolated swelling spots (bulges) or lines (wrinkles) on the retina were observed in 68% of the 198 treated eyes. Green fluorescence was also observed at these areas (Fig. 4B). Histological examination showed that the retina was thickened and staining with anti-Islet1 and anti-neurofilament antibodies revealed that the differentiation of ganglion cells had expanded to the surface layer at these places (Fig. 4C). In 32% ($n = 198$) of the Pax6(−5a)-treated eyes, an embankment-like structure swelled out on the retina. In addition, several fibres (10–100 μm in length) grew out into the vitreous cavity (Fig. 4D). Sections were stained with specific antibodies for Islet1, a homeodomain-containing transcription factor that is expressed in the ganglion cells in the developing retina (30), and neurofilament protein, an intermediate filament protein specific to retinal neurons (31). The immunohistochemistry suggested that the fibres in the vitreous cavity were nerve bundles derived from ganglion cells (Fig. 4E). These abnormal structures may be caused by the unbalanced growth and differentiation of the retina, because the nerve fibres extended onto the retinal surface and formed additional layers on the retina.

When the Pax6(+5a) isoform was misexpressed instead of Pax6(−5a), more dramatic changes were observed inside the enlarged eyes 3–7 days after electroporation (HH stages 28–35). Of the 187 treated eyes, 6% had a wall-like structure protruding into the vitreous cavity, which was shown to be a

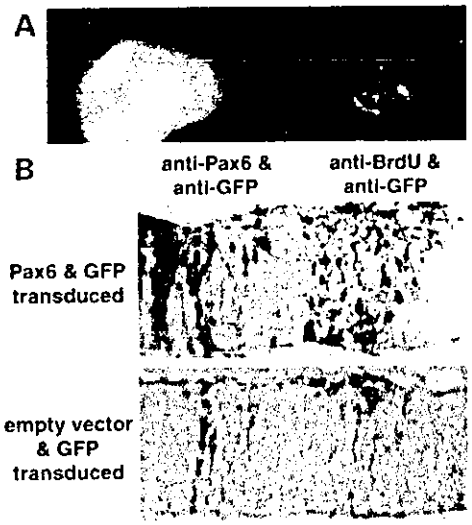

Figure 3. Early changes in the developing chick eye induced by the electroporation of Pax6(−5a). Constructs expressing Pax6(−5a) and GFP were electroporated into the right eye primordium of HH stage 16 chick embryos ($n = 5$). (**A**) Twelve hours after electroporation (HH stage 18), expression of GFP in the right eye was examined using fluorescence microscopy. (**B**) Sections double-immunostained with anti-GFP (violet) and anti-Pax6 (brown) and anti-GFP (violet) and anti-BrdU (brown) antibodies show the expression of the electroporated GFP and Pax6(−5a) constructs and the pronounced proliferation of the retinal progenitor cells around the electroporated area, but transduction of empty vector, pCAGGS-GFP or both constructs did not induce any change ($n = 5$ for each). (bar scale 20 μm). Transduction of the Pax6(+5a) isoform had a similar effect on eye development at these stages ($n = 5$; data not shown).

folded retina by histological analysis (Fig. 4G and H) and 42% showed thick stick-like structures protruding from the retina into the vitreous cavity (Fig. 4I and J). These protruding structures were very long and some even approached the lens on the opposite side. Cross sections of these protrusions were subjected to *in situ* hybridization with probes specific for *Musashi*, which encodes a neural RNA-binding protein highly enriched in neural precursor cells (32), *Six3*, a homologue of *Drosophila* homeobox gene *sine oculis*, that is expressed in inner and outer nuclear layers (33), and *Rx*, a paired-class homeobox gene, which is expressed in the inner nuclear layer, presumably bipolar cells of the developing retina (34). Immunohistochemical staining with anti-ISlet1 and anti-neurofilament antibodies was also performed (Fig. 4K). These analyses suggested that the tubular structures consist of well-differentiated retinal layers, which include nerve fibres, ganglion cells and developing inner and outer nuclear layer cells, with an outer surface layer of nerve fibres and an inner surface of photoreceptor cells. These tubular and fold structures suggest that the horizontal overgrowth of the neural retinal layer occurred at the regions where Pax6(+5a) was misexpressed. As space was limited even in the enlarged eyeball, the regional expansion of the cells seemed to push the retinal layer up into the vitreous cavity. Such drastic outgrowths that contain all retinal cell types was never obtained when Pax6(−5a) was misexpressed. Electroporation of the empty vector alone or the pCAGGS-GFP or both constructs did not induce any phenotypic changes. Thus, we conclude that the Pax6(+5a) isoform can induce horizontal overgrowths of the retina that protrude into the vitreous cavity. Of the 187 treated eyes, 34% of the Pax6(+5a)-treated eyes, which showed protrusion of the retina, became significantly larger than untreated control eyes (Fig. 4F). Although we have reproducibly generated this protruding retina by electroporating at HH stages 16–24, such morphological alterations were not induced when the electroporation was performed at later stages. Transduction of Pax6(−5a) or Pax6(+5a) using an adenoviral vector or electroporation using smaller amounts of plasmid DNAs caused similar, although somewhat weak phenotypic changes (data not shown). The incidence of the Pax6(−5a)- and Pax6(+5a)-dependent eye architectural changes at each stage is available in Supplementary Material.

We next examined the distribution of photoreceptor cells in the protruding retinal structures. Embryos were allowed to develop just before hatching (HH stages 40–45) and then analyzed. Some lectins, including peanut agglutinin and wheat germ agglutinin, specifically stain cone photoreceptor cells (35), which are normally condensed at the visual streak in the posterior portion of the chick eye (Fig. 5A and B e region). Histochemical examination revealed that the cone cells were detectable in the folded retina not only near the visual streak (d region) but also in the peripheral portion (c region) where lectin-staining is normally negative as observed in an unaffected peripheral portion (b region). Colour opsins are components of cone cells (2,3,36). RT–PCR showed that three types of colour *opsins* were expressed in the peripheral and posterior portions of the folded retina (c and d regions) at a similar level as in an unaffected region in the posterior portion of the retina (e region), and more intensely than an unaffected region of the peripheral portion of the retina (b region) (Fig. 5D). In contrast, the expression level of *rhodopsin*, a component of rod cells, was high in the peripheral areas and low in the visual streak (2,3). The peripheral portion of the folded retina (c region) exhibited *rhodopsin* expression at a similar level as the control peripheral area, whereas the expression level in the affected region in the posterior portion of the retina (d region) was similar to that in the visual streak (e region). These results suggest that the differentiation of retinal cells is highly promoted in the protruding retina to the level seen in the visual streak with regard to both the layer structure and the density of cone cells.

Effect of missense mutations of the *Pax6* gene on retinal overgrowth

To understand which element or structure of Pax6 is important for inducing the retinal overgrowth observed, we introduced several mutations into the Pax6 PD: (a) the R26G mutation in the NTS (25), (b) the R128C mutation in the CTS (4) or (c) the V54D mutation in exon 5a (5). The transactivation potentials of wild-type and mutant Pax6 with or without exon 5a have been assayed previously (5,22) or in this study using reporter genes containing P6CON or 5aCON, which are consensus binding sites for the (−5a) and (+5a) isoforms, respectively. As summarized in Figure 6A, the NTS in Pax6(−5a) wild-type is responsible for P6CON-binding,

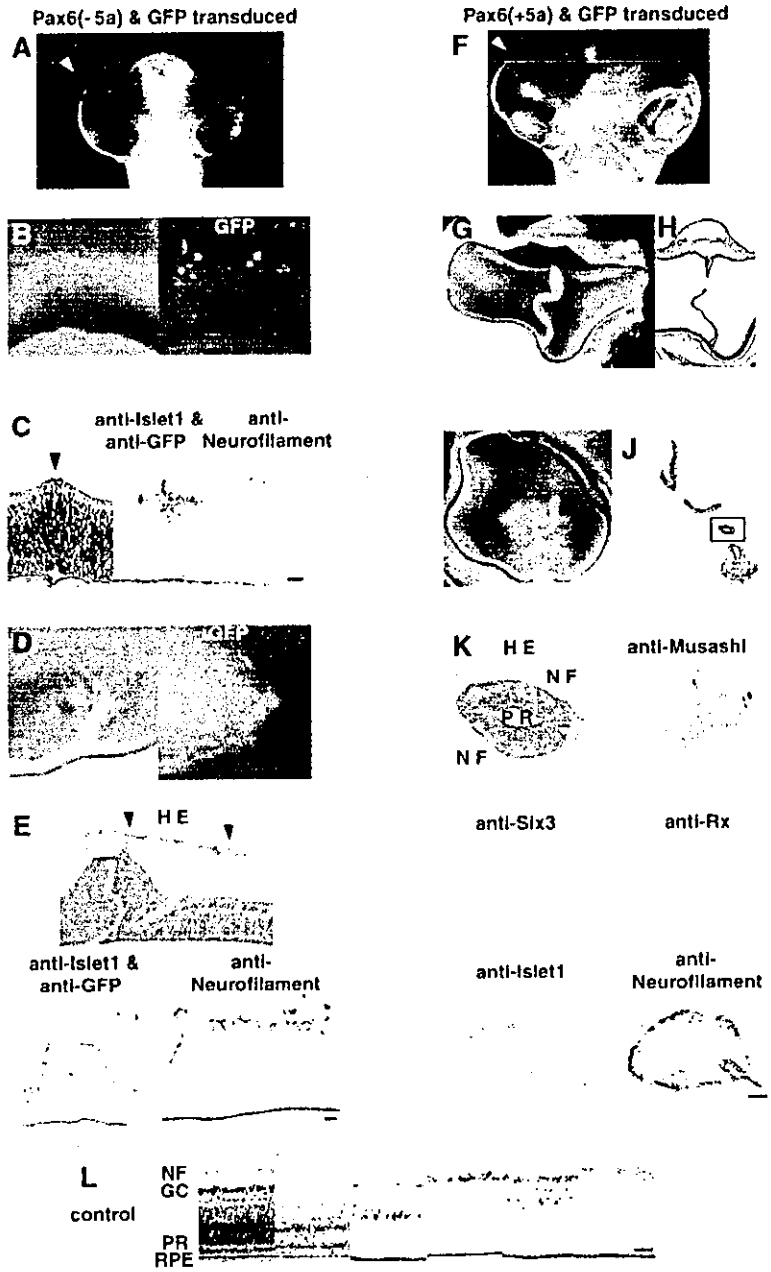

Figure 4. Later changes in the developing chick eye induced by electroporation of Pax6(−5a) (A–E) or Pax6(+5a) (F–K) together with GFP. (A–C) A Pax6(−5a)-transduced embryo at HH stage 30. (A) The frontal view shows an enlarged eye (arrowhead). (B) The inside views show several areas of swelling on the retinal layer with green fluorescence (the right panel, matched field). (C) Sections stained with HE, anti-islet1, anti-GFP and anti-neurofilament antibodies. Islet1 (brown) and GFP (violet) were double-stained. Ganglion cells (arrowhead) excessively differentiated in the surface layer of the thickened retina where the electroporated GFP constructs is expressed (bar scale 20 μm). (D, E) A Pax6(−5a)-transduced embryo at HH stage 34. (D) A view of the split eyeball shows embankment-like swelling from the retina with numerous fibres with green fluorescence (matched field). (E) Numerous fibres grow from the embankment-like retina into the vitreous cavity (arrowheads). Sections immunostained with anti-ISlet1 (brown), anti-GFP (violet in the left lower panel) and anti-neurofilament (brown) antibodies show expression of the electroporated constructs and ectopic growth of the nerve bundles from the retina (bar scale 20 μm). (F–H) A Pax6(+5a)-transduced embryo at HH stage 34. (F) A frontal view shows a significantly enlarged eye that breaks through the eyelid skin (arrowhead). Views of the split eyeball (G) and section with HE staining (H) show that the retina overgrows to show fold structure. (I–K) A Pax6(+5a)-transduced embryo at HH stage 36. Views of the split eyeball (I) and section with HE staining (J) show that the retina overgrows into stick structure. GFP expression was weak and could not be detected in the aberrantly growing tissues. (K) Analysis of the boxed region of the section indicated by (J) by *in situ* hybridization using probes specific for *Musashi, Six3* and *Rx* and immunohistochemistry with anti-islet1 and anti-neurofilament antibodies. These analyses suggest that the aberrantly growing tissues in the Pax6(+5a)-transduced eyes are composed of well-differentiated retina layers (bar scale 20 μm). NF, nerve fibres; PR, photoreceptors. (L) A portion of the posterior retina normally developing at a corresponding stage is illustrated for comparison. NF, nerve fibres; PR, photoreceptors; RPE, retinal pigment epithelium (bar scale 20 μm).

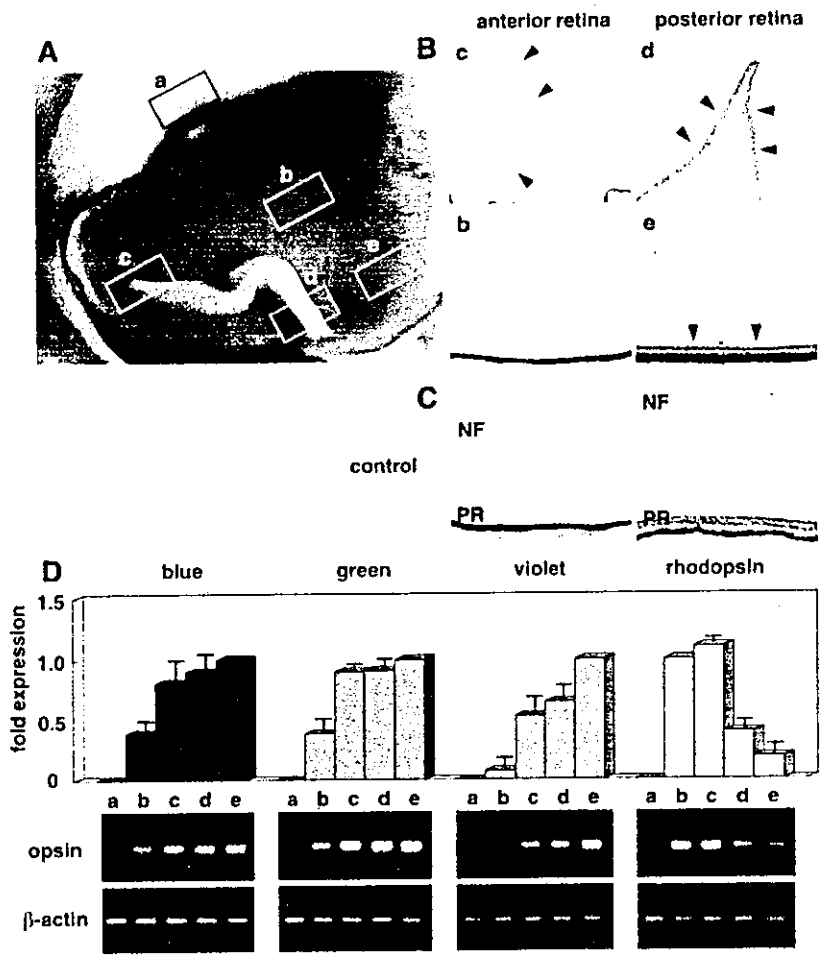

Figure 5. Differentiation of photoreceptor cells in the extruding and folded retina induced by electroporation of Pax6(+5a) at HH stage 18. **(A)** A view of a split eyeball at HH stage 45 shows the folded retina. Five areas were examined: (a) the cornea, (b) an unaffected region in the peripheral portion of the retina, (c) a peripheral portion of the folded retina, (d) a posterior portion of the folded retina and (e) an unaffected region in the posterior portion of the retina including the visual streak. **(B)** Staining with peanut agglutinin shows the presence of cone photoreceptor cells in the c region as well as in the d and e regions (arrowheads). **(C)** A portion of the retina normally developing at a corresponding stage is also illustrated for comparison. NF, nerve fibres; PR, photoreceptors (bar scale 20 μm). **(D)** Semi-quantitative RT–PCR demonstrates the expression of three colour *opsins* (*blue, green* and *violet*) and *rhodopsin* in the various regions. The bar graphs are shown as mean ± SD ($n = 3$) of ratio of expression in a–d region to that in e region (blue, green and violet *opsins*), or ratio of expression in a or c–e region to that in b region (*rhodopsin*). The photograph of RT–PCR analysis under the bar graph is representative of three independent experiments using six treated eyes.

while in Pax6(+5a) wild-type, the insertion of 14 amino acids encoded by exon 5a into the NTS abolishes its NTS P6CON-binding activity and unmasks the CTS 5aCON-binding ability. The R26G mutation in the NTS strongly impairs the NTS- and P6CON-mediated transcriptional activation of Pax6(−5a) and increases the CTS- and 5aCON-mediated transcriptional activation of Pax6(+5a). In contrast, the R128C mutation in the CTS abolishes the CTS- and 5aCON-mediated transcriptional activation of Pax6(+5a), and hyperactivates the NTS- and P6CON-mediated transcription activation of Pax6(−5a). The V54D mutation in exon 5a has a weak inhibitory effect on the CTS-and 5aCON-mediated transcriptional activation, but increases the NTS- and P6CON-mediated transcriptional activation. Thus, it has been proposed that the two subdomains negatively regulate each other, and exon 5a thus appears to function as a molecular switch that determines target gene specificity. When these mutants were misexpressed in the primordial retina of HH stages 16–30 chick embryos, only Pax6(+5a) R26G and Pax6(−5a) R128C induced a phenotypic change. Retinal overgrowth was observed in 34% and 26% of the eyes that had received Pax6(+5a) R26G ($n = 54$) and Pax6(−5a) R128C ($n = 56$) respectively, although the observed phenotypic changes were less significant than those induced by the respective wild-type Pax6 isoforms. Morphological changes induced by Pax6(+5a) R26G were more drastic than those induced by Pax6(−5a) R128C. Retinal swelling and string- and stick-like structures induced by Pax6(+5a) R26G (Fig. 6B), and fibres induced by Pax6(−5a) R128C (Fig. 6C) are shown as examples. The incidence of eye architectural changes by transduction of